Development of a protocol utilizing single-cell analysis for the differentiation of human iPSCs into SOX6+ midbrain dopaminergic neurons.

Guochang Lyu[1]*, Roberto Garcia-Swinburn[1]*#, Judith C. Kreutzmann[1,2] , Anqi Xiong[1], Rika Kojima[2], Carmen Abaurre[1], Chiara Tremolanti[1], Sandra Gellhaar[1], Per Uhlén[1], Per Svenningsonn[2], Gonçalo Castelo-Branco[1], Onur Dagliyan[1]#, Carmen Salto[1], Ernest Arenas[1]†

[1]Department of Medical Biochemistry and Biophysics, Karolinska Institutet, 171 77 Stockholm, Sweden

[2]Department of Clinical Neuroscience, Karolinska Institutet, 171 76 Stockholm, Sweden

*These authors contributed equally

Correspondence to roberto.garcia.swinburn@ki.se or onur.dagliyan@ki.se

† Deceased 15/09/2024

ABSTRACT

Parkinson's disease (PD) is a neurodegenerative disorder characterized by the loss of midbrain dopaminergic (mDA) neurons in the substantia nigra, leading to motor symptoms. Current pharmacological treatments are insufficient in halting disease progression, making cell therapy a promising alternative for replacing lost neurons. Advances in stem cell research have enabled the generation of mDA progenitors from human pluripotent stem cells (hPSCs), demonstrating success in preclinical models and clinical trials. However, challenges such as dyskinesias from non-mDA contaminations, graft rejection, and the need for more specific cell types persist. This study focuses on utilizing single-cell multiomic and transcriptomic data to design mDA progenitor differentiation protocols, aiming to generate more specific subtypes of mDA neurons, particularly those vulnerable to degeneration in PD. By refining the protocol with enhanced ventralization and prolonged Wnt activation, we achieved improved midbrain patterning, cell viability, and the accelerated generation of SOX6-expressing mDA neurons *in vitro* with proven therapeutical properties in grafted hemiparkinsonian mice models. This approach aims to present a protocol designed using single-cell analysis to enrich the most PD-affected mDA neuron populations, offering potential for better cell modelization, and more targeted cell replacement therapies.

INTRODUCTION

Parkinson's disease (PD), the second most prevalent neurodegenerative disorder, presents significant challenges in treatment and patient quality of life. The progressive degeneration of midbrain dopaminergic (mDA) neurons in the substantia nigra pars compacta (SNpc), which primarily project to the dorsal striatum, leads to the loss of dopaminergic input to the striatum and results in the characteristic motor symptoms of PD (Poewe et al., 2017). Although advances in pharmacological therapies have been made, these treatments are often insufficient in halting disease progression or restoring lost neuronal function in later stages (Brichta et al., 2013). Cell

therapy offers a promising alternative, with the potential to replace the damaged or lost DA neurons critical to Parkinson's pathology (Björklund & Parmar, 2021).

Advances in stem cell research and a deeper understanding of midbrain development have enabled the production of mDA progenitors from human pluripotent stem cells (hPSCs) for transplantation (Doi et al., 2014; Kim et al., 2021; Kriks et al., 2011; Nishimura et al., 2022). Success in preclinical models has led to the development of clinical-grade mDA progenitors for PD clinical trials (Kirkeby et al., 2023; Piao et al., 2021; Schweitzer et al., 2020; Takahashi, 2020). Furthermore, phase I/II clinical trials have recently been completed using hPSCs demonstrating safe outcomes for these therapies, paving the way for future medical use of hPSCs (Tabar et al., 2025; Sawamoto et al., 2025).

As a result, there has been a growing focus on assessing the quality and composition of cells derived from hPSCs. Research is underway to better define and molecularly characterize human mDA neuron development at the single-cell level (Braun et al., 2023; Manno et al., 2016). These studies have provided detailed analyses of the cellular composition and molecular features of individual cell types in hPSC-derived midbrain preparations (Manno et al., 2016; Nishimura et al., 2022; Tiklová et al., 2020; P. Xu et al., 2022).

However, challenges remain in the effectiveness of cell-based therapies, including complications like dyskinesias reported in fetal tissue transplants. These have been reported years after transplantation and are believed to result from serotonergic neuron contamination within the graft (Greene et al., 2021). Another major challenge is graft rejection by the host, typically addressed through pharmacological immunosuppression. The use of human-induced pluripotent stem cells (hiPSCs) presents a potential solution by enabling the generation of patient-specific neurons, thereby overcoming immune rejection (Schweitzer et al., 2020).

Single-cell transcriptomics has revealed significant diversity within mDA neurons in the adult human SNpc, categorizing them into three major classes based on the expression of SOX6, CALB1, and GAD2 (Kamath et al., 2022; Siletti et al., 2023). These classes are also detectable during human mDA neuron development (Braun et al., 2023). Additionally, advances in single-cell technologies have now made it possible to assess developmental epigenetics by the use of ATAC-seq in developing human midbrain (Mannens et al., 2024). To better understand how to generate specific mDA neuron subtypes, we analyzed multiomic data from established protocols to identify approaches that enrich for the SOX6 class, as a $SOX6^{+}AGTR1^{+}$ subpopulation has been linked to increased vulnerability to neurodegeneration in PD in humans and parkinsonian models (Kamath et al., 2022; Salmani et al., 2024).

In summary, we initially used a simplified mDA neuron differentiation protocol based on key developmental components identified through single cell multiomics. This protocol was reproducible across distinct iPSC lines. However, insights from molecular phenotyping indicated that the resulting phenotypes were not maintained at later stages, suggesting insufficient patterning, leading us to modify the protocol. A new protocol involving enhanced ventralization and prolonged Wnt activation improved midbrain patterning, increased cell viability, and generated more mature mDA neurons with higher expression levels of *OTX2*, *EN1* and *SOX6* compared to the original protocol. Furthermore, we tested *in vivo* differentiation of

our cells in hemiPD rodent models, achieving a high number of $SOX6^+$ mDA neurons with effective motor recovery.

While various differentiation protocols exist, many lack specificity to target the DA neuron subtypes most vulnerable to degeneration in PD. Our work aims to address this gap by identifying key developmental factors using multiomic data and evaluating a novel protocol to enrich *in vitro* the mDA neuronal population most affected by Parkinson's disease and further validate as proof-of-concept in *in vivo* PD models.

MATERIAL AND METHODS

Cell lines

KOLF 2.1J cell line was obtained through collaboration with the Aligning Science Across Parkinson's (ASAP) consortium. Genotypes, pluripotency, and mycoplasma infection were routinely assessed before starting new experiments. Applied iPSC lines were adapted to grow on Laminin 521 (Biolamina, LN521)-coated plates and maintained in Essential 8 Flex media (Thermo Fisher Scientific) at 37ºC, 5% CO_2, until starting differentiation. The medium was changed daily, and cells were passaged at 70% confluency using TrypLE™ Select Enzyme (Thermo Fisher Scientific) at a 1:20 ratio. When thawing and replating, 10 µM Rho-associated protein kinase (ROCK) inhibitor (Y-27632) (Tocris) was added into the culture media overnight.

Midbrain dopaminergic neuron differentiation

Prior to the mDA differentiation, adapted iPSC cells were seeded at a density of 200,000 cells/cm^2 onto vessels coated with Geltrex (Life Technologies) and Laminin-511 (Biolamina, LN511), and maintained in Essential 8 Flex media (Thermo Fisher Scientific) for expansion. The differentiation protocol should be initiated when the cells reach approximately 80% confluency. Cultured cells will be kept in Neurobasal/N2/B27 (Life Technologies) medium and 2 mM L-glutamine (Invitrogen), along with various supplements for the first stage of the protocol. From day 0 to day 3, the culture medium was conditioned with 250 nM LDN193189 (Stemgent), 10 µM SB431542, 2 µM Purmorphamine, and 0.7 µM CHIR99021 from day 0 to day 3, with the inclusion of 10 µM Y27632 (Tocris Bioscience) during the first 24 hours. Boosted CHIR9901 (7.5 µM) was administered from day 4 to day 10, while LDN193189, SB431542 and Purmorphamine were withdrawn after day 7. From day 10 to day 28, cells were switched to the differentiation media: Neurobasal/B27/L-Glu media supplemented with 20 ng/mL brain-derived neurotrophic factor (BDNF, R&D Systems), 20 ng/ml glial cell line-derived 455 neurotrophic factor (GDNF, R&D Systems), 1 ng/ml transforming growth factor type b3 (TGFb3, R&D Systems), 0.2 mM ascorbic acid (Sigma), 0.2 mM Dibutyryl cAMP (Sigma). On day 11 and 16, the resulting cells were dissociated into single cells, replated at a density of 800,000 cells/cm^2 onto plates coated with LN511 and polyornithine/LN511 respectively, and treated with 10 µM Y27632 for 48 hours. To promote neurogenesis, the mDA differentiation media was supplemented with 10 mM DAPT (Sigma) from day 12-28. The small molecule GW3965 (10 µM) was administered from day 12 to day 15, followed by a cocktail of small molecules consisting of 1 µM PD0325901 and 5 µM SU5402 (Sigma), from day 16 to day 21.

Immunocytochemistry

121 Progenitor cells at different stages were seeded in a 96-well plate at a density of about 300,000
122 cells per well for the intended cell culture purposes. Harvested cells were fixed by 4%
123 paraformaldehyde (PFA) for 20 min at 4ºC, and then pre-incubated by 5% donkey serum in
124 phosphate buffered saline containing 0.3% Triton X-100 (PBST) for 1 hr. The samples were
125 incubated with primary antibodies at 4ºC overnight. The samples were incubated with either
126 Alexa488 or Alexa555 or Alexa647-conjugated secondary antibodies (Thermo Fisher Scientific)
127 for 30 min and then were incubated with 4',6-diamidino-2-phenylindole (DAPI) for 15 min. The
128 primary antibodies were used as follows: CORIN (rat, 1:1,000, R&D Systems, MAB2209), DCX
129 (goat, 1:500, SantaCruz, sc-8066), EN1 (mouse 1:50, DSHB, 4G11), FOXA2 (goat, 1:500, R&D
130 Systems, AF2400), GIRK2 (rabbit, 1:400, Alomone, APC006), LMX1A (rabbit, 1:4,000, Millipore,
131 AB10533), LMO3 (goat, 1:200, SantaCruz, sc-82647), MAP2 (mouse 1:1,000, Sigma, M4403),
132 NURR1 (rabbit, 1:500, SantaCruz, sc-990), OTX2 (goat, 1:1,000, R&D Systems, AF1979), TH
133 (rabbit, 1:1,000, Millipore, AB152), TH (mouse, 1:500, ImmunoStar, 22941), and TH (sheep,
134 1:500, Novus, NB300). Mounted cells were further visualized using Zeiss LSM880 or 980.
135 Quantification of images was performed using QuPath (Bankhead et al., 2017) by generating a
136 "single measurement classifier" or "composite classifier" for positive or double-positive cells
137 respectively.

138 **Calcium imaging**

139 The 35mm culture dishes were loaded with the Ca2+-sensitive fluorescence indicator Fluo-
140 4/AM (5 μM; Invitrogen, USA) and Pluronic F-127 (0.625%, ThermoFisher Scientific) and
141 incubated for 30 min at 37ºC in Krebs-Ringer buffer, containing: NaCl (119 mM), KCl (2.5 mM),
142 NaH2PO4 (1 mM), CaCl2 (2.5 mM), MgCl2 (1.3 mM), HEPES (20 mM) and D-Glucose (11 mM),
143 with pH adjusted to 7.4. Dishes were washed twice and Ca2+-measurements were performed in
144 Krebs-Ringer buffer at 37ºC on a confocal spinning disk microscope (Nikon CrEST X-Light V3)
145 equipped with a 20x Air lens. Excitation was assessed at 480 nm at a sampling frequency of 1
146 Hz. The equipment was controlled with, and data was acquired using the Nikon NIS-Elements
147 software. FIJI, MATLAB (R2020b, MathWorks, USA) and FluoroSNNAP
148 (https://github.com/tapan-patel/FluoroSNNAP) were used to process and analyze the data.

149 **Single cell sequencing libraries preparation and data processing**

150 A total of 5 samples (DIV 11, 16, 28, 42, and 56) from KOLF2.1J mDA neuron cultures generated
151 with the optimized protocol were collected for time-course multiomic analysis (ATAC + Gene
152 Expression); while 3 samples (DIV 14, 16, and 28) from the new protocol trial of KOLF2.1J mDA
153 differentiation were collected for single-nuclei transcriptomic profiling. All 8 samples were
154 prepared with demonstrated protocols (10x Genomics) and the resulting Fastqc files were
155 processed through the 10X Genomics Cellranger pipeline (Zheng et al., 2017), while 5 multiomic
156 libraries were aligned to the hg38 reference genome using Cellranger-arc default settings
157 (Satpathy et al., 2019). Resulting transcriptomic and epigenomic data from individual samples
158 were combined by projects using the 'aggr' function in Cellranger or Cellranger-arc, without
159 normalization applied. Objects produced with Seurat V4.4.0 was employed to accommodate
160 aggregated count matrix (Stuart et al., 2019), with the fragment files specifically integrated into
161 Signac v1.9.0 chromatin assays (Stuart et al., 2021). Quality metrics for gene expression and
162 peak accessibility, such as mitochondrial ratio, cell cycle score, nucleosome signal, and
163 Transcription Start Site (TSS) enrichment, were thereafter calculated to determine quality

control cutoffs. Depending on sample quality, following thresholds were applied for downstream analysis: a maximum of 300,000 and a minimum of 1,000 ATAC counts per cell, a maximum of 25,000 and a minimum of 600 RNA counts, at least 250 genes detected, a maximum nucleosomal signal of 1.5, TSS enrichment of at least 2, and mitochondrial content no higher than 15%. These cutoffs reduced the cell count by less than 20% without significantly affecting clustering downstream. Peak calling was performed with MACS2 v2.2.9 using the aggregated fragments file (Y. Zhang et al., 2008), and those mapped to non-standard chromosomes or overlapping hg38 genome blacklist regions were excluded. DoubletFinder v2.0 was applied to identify doublets in gene expression data by flagging instances with a high resemblance to artificial neighbors in gene expression space (McGinnis et al., 2019). AMULET (ATAC-seq MULtiplet Estimation Tool) was additionally utilized to detect potential multiplets in snATAC-seq datasets by enumerates regions with greater than two uniquely aligned reads across the genome (Thibodeau et al., 2021). All predicted doublets were removed from the downstream analysis. After merging high-quality cells from the relevant projects, count data was normalized using SCTransform V2 function with regression out of mitochondrial or cell-cycle genes. The top 2,000 most variable genes were initially identified through variance-stabilizing transformation, along with 95% of the most frequent peaks in multiomic datasets, as a part of the significant feature selection process. Subsequent dimensionality reduction was performed using the principal components analysis (PCA), in which the top 30/40 principal components were chosen from the elbow plot to represent most of the diversity of datasets. For single-nuclei ATAC-seq datasets, singular value decomposition (SVD) was performed with the top 25 of the Latent Semantic Indexing (LSI) layers to reduce the dimensions of the most common peaks. Notably, the first LSI component was excluded from downstream analysis as it often captures sequencing depth (technical variation) rather than biological variation. Putative clusters were identified by a spiking neural network (SNN) modularity optimization-based clustering algorithm, and the optimal resolution of clustering was determined by iterating over different resolution for the most stable segregation. Finally, the calculated nearest-neighbor graph was projected to two dimensions to visualize the distribution of instances by representing with uniform manifold approximation and projection (UMAP). To accurately identify and interpret cell states in vitro, we leveraged combined manual cell type annotation using cluster-specific marker genes (Clarke et al., 2021; Zhou et al., 2019), with automatic annotation methods using reference datasets that characterize first-trimester developing human brain (Braun et al., 2023; C. Xu et al., 2023). Initially, a label transfer was performed with Celltypist (Conde et al., 2022) and 'TransferData' function in Seurat to automatically classify selected dataset with cell type labels from the reference dataset, based on the similarity of query gene expression profiles to selected anchors in the reference dataset. The identity of each cell will be determined by the highest prediction score, and for stringent comparison, cells with a prediction score below 0.51 will be excluded from downstream analysis. After data trimming and reclustering, a manual cluster-based annotation was performed, using both expression levels of canonical midbrain development marker genes and top 50 upregulated genes identified by the 'FindAllMarkers' function. These upregulated genes were used for pathway and biological process enrichment analysis via Metascape (Zhou et al., 2019), and the top-ranked terms were used to refine annotations and determine cell subtypes or states. To reconstruct the putative trajectory of mDA differentiation in vitro, we employed Monocle3 (Trapnell et al., 2014) and scVelo (Bergen et al., 2020; Gayoso et al., 2024) to infer pseudo- and latent-temporal

ordering of cells using default parameters. The root of trajectory for pseudotime analysis was set as ProgFP or NbM at the earliest timepoint.

Animals

Healthy female adult (8-12 weeks old) C57BL/6N-Rag2Tm1-IL2rgTm1-SirpaNOD/Rj (B6RGS) mice were purchased from Janvier Labs. Groups of 5 animals were housed in ventilated cages under a 12 h light-dark cycle with food (standard chow) and water ad libitum at 20-22 ºC and 50-55% humidity. All surgical procedures followed aseptic techniques, and for post-surgical recovery, additional Dietgel Recovery (Scanbur) and food pellets were supplied on the cage floor. All procedures were approved by the local ethical committee (Stockholms djurforsoksetiska namnd) and followed the EU directive 2010/63/EU under the ethical permit of Ernesto Arenas Cases and Sandra Gellhaar (12265-2021; 2-3143/23; 2-3595/24; 2-3147/24).

6-OHDA mouse model

B6RGS mice were acclimatized 2-3 weeks before surgery to the animal facility and the researcher and to a recovery diet 2-3 days before surgery. For 6-hydroxidopamine (6-OHDA) lesions (or sham), animals were injected analgesia (Carprofen 5mg/kg + Buprenorphine 0.1 mg/kg) 15 minutes before isoflurane induction (4%). Animals were anesthetized at 1-2% isoflurane in air and injected intracranially (ICR) using a Neurostar Robotic Stereotaxic Frame equipped with a 10 µl syringe with 33G blunt needle (Hamilton) 1 µl of 6-OHDA 3.6 µg/ µl in sterile ascorbic acid/saline 0.02% (or sham vehicle) in the right medial forebrain bundle [respect to Bregma: AP -1.2 mm, ML +1.2 mm, DV -5.0 mm] at a flow of 0.2 µl/min, raising the needle 500 µm for 3 minutes. The needle was left inside for 2 additional minutes. Animals were placed in warm cages (28 °C) between 3 days and 1 week for better recovery and rehydrated with Ringer Acetate solution if weight decreased by 5%. 6-OHDA hemiparkinsonism was confirmed by amphetamine-induced rotation. Briefly, 4 weeks after the lesion, mice were injected intraperitoneally with d-amphetamine in saline (5 mg/kg). 10 minutes after injection, the mice were recorded for 30 minutes inside a 15 cm wide cylinder in dark conditions, and the number of net ipsilateral rotations (ipsilateral-contralateral) per minute in active movement was calculated using Ethovision XT 17. Mice are considered hemiparkinsonian if the values are >6 rotations/minutes.

hiPSC transplant

HemiPD-confirmed mice of healthy weight (22-30 g) were randomly selected for ICR hPSC injection in the right striatum [respect to Bregma: AP +0.5 mm, ML +2 mm, DV -3.5 mm]. Analgesia and anesthesia were followed as above. For ICR transplants, 2 µl of 100.000 ± 20.000 hPSCs/µl in Neurobasal medium was injected to achieve 200.000 hPSC transplants. For cell injection, the Neurostar robot was coupled with a 10 µl syringe with a 27G sharp syringe. A flow of 0.5 µl/min was used, and the needle remained for 5 additional minutes. Cells were injected between 1-6 hours after thawing.

Amphetamines-induced rotations

Mice were analysed once a month until endpoint was reached. Mice were injected intraperitoneally with d-amphetamine in saline (5 mg/kg). 10 minutes after injection, the mice were recorded for 30 minutes inside a 15 cm wide cylinder in dark conditions, and the number of

net ipsilateral rotations (ipsilateral-contralateral) per minute in active movement was calculated using Ethovision XT 17.

Pole test

Animals were placed facing upwards on the top of a 20 cm vertical pole. The time to climb down was counted starting when the mouse rotates facing downwards. Animals were trained for a minimum of 2 days before testing day.

Cylinder wall

Animals were placed inside a 12 cm diameter glass cylinder in red light and quiet conditions. For 15 minutes, animals were recorded and videos were analysed at x8 speed. Unilateral contacts were counted.

Tape removal test

A green adhesive tape 2x3 mm was placed on each paw individually. The time it took to remove the tape was counted, beginning when the mouse recognized it and ending when it was removed from the paw. Net contralateral time (ipsilateral-contralateral) was calculated to better visualize and eliminate external factors. Before testing day, animals were trained for a minimum of 2 days.

Immunohistochemistry

Animals were terminally anesthethised with pentobarbital and then perfused intracardially with 50 ml of pH-corrected PBS1X followed by 50 ml of formaldehyde 4 % (FA) both at a flow of 9 ml/min. Brains were extracted and placed in FA overnight, after which they were placed in sucrose 30%/PBS solution at 4ºC for 2-3 days. After, brains were kept at -80ºC.

Brains were equilibrated at -20ºC for 4 hours before slicing. Samples were sliced in series at -20ºC at 20 µm using a Cryostar NX70 (Epredia) and stored for further use at -20ºC in cryoprotective solution (Ethylenglycol 30%,Glycerol 30%,PBS1X). A total of 5 brains were processed.

Samples were stained using free-floating protocols. Briefly, 2 series of 5 minutes of PBS1X, followed by 15 minutes of PBS-TritonX 0.3% (PBTx0.3%), then 2 series of 5 minutes of PBTx0.1%. Samples were blocked for 1 hour with blocking solution (BSA 1 mg/ml, Normal Donkey Serum 5%, PBTx0.1%) and incubated o/n at 4ºC with primary antibody diluted in blocking solution. Primary antibody was washed with 2 series of 5 minutes PBTx0.1% and samples were incubated for 4 hours with secondary antibody diluted in blocking solution and washed twice for 5 minutes with PBS1X. Tissue was counterstained with 4',6-diamidino-2-phenylindole (DAPI, Sigma, D9542) 1:1000 in PBS1X for 10 minutes and then washed twice for 5 minutes with PBS1X. Stained samples were mounted on Superfrost Plus slides (Epredia) and Fluoromount-G mounting medium (00-4958-02, Thermo Scientific). Primary antibodies used were STEM121 (mouse, 1:1000, Tanaka Bio, Y40410), TH (rabbit, 1:1000, Pelfreeze, P4010; sheep, 1:250 Pelfreeze, P60101), HuNu (mouse, 1:1000, Millipore, MAB1281), SOX6 (rabbit, 1:200, Abcam, ab30455), ALDH1A (rabbit, 1:500, Atlas Antibodies, HPA002123), AGTR1 (rabbit, 1:100, Invitrogen, MA5-56587), Calbindin-1 (rabbit, 1:200, Invitrogen, PA5-85669), LMX1 (rabbit, 1:100, Millipore, AB10533), FOXA2 (rabbit, 1:200, Cell Signaling, 3143S), NR4A2 (rabbit, 1:500,

290 Invitrogen, PA5-78097), PITX3 (rabbit, 1:100, Invitrogen, 35-2850), DAT (rat, 1:250, Abcam,
291 ab5990), GIRK2 (rabbit, 1:500, Alomone Labs, APC006), VMAT2 (rabbit, 1:500, Sigma-Aldrich,
292 AB1598P), DDC (rabbit, 1:500, Novus Biological, NB300-252), Ki67 (rabbit, 1:200, Abcam,
293 ab15880), SOX2 (goat, 1:200, R&D Systems, AF2018). All secondary antibodies were from
294 Invitrogen, donkey as host and conjugated with Alexa Fluor 488, 555 or 647. Images were
295 captured either with laser confocal microscope Zeiss LSM800 or high-throughput
296 epifluorescence microscope Zeiss Axioscan. Quantification of images was performed using
297 QuPath (Bankhead et al., 2017) by generating a 'single measurement classifier' or 'composite
298 classifier' for positive or double-positive cells respectively.

299 **Single-nuclei RNA sequencing of grafts and data analysis**

300 Animals were euthanized by cervical dislocation and brains were promptly extracted and flash-
301 frozen in dry-ice chilled isopentane for 10-15 seconds. Flash-frozen brains were stored at -80 °C
302 until graft extraction. A total of 3 brains with grafts were processed.

303 On the day of nuclei extraction, brains were equilibrated to -20ºC and sliced in -20ºC cooled
304 chambers. Brain matrices were used to stabilize the brain, and 1 mm-thick slices for a total of 4
305 (2 before the graft implant location and 2 after) were cut using chilled razors. 1 mm punches of
306 each slice of the dorsal striatum were extracted using 1 mm biopsy-punchers (49101, PFM
307 Medical).

308 Nuclei were dissociated using the 10X Genomics Chromium nuclei extraction kit (1000494)
309 using manufacturer's instructions. For better extraction, eppendorfs used for tissue
310 dissociation were coated with BSA 1% o/n at 4ºC, briefly washed with filtered sterile PBS1X
311 before procedure. 10X Genomics Chromium GEM-X Single Cell 3' Kit v4 (1000691), Chromium
312 GEM-X Single Cell 3' Chip Kit v4 (1000690) and Dual Index Kit TT Set A (1000215) were used for
313 GEM generation using manufacturer's instructions with the 10X Controller iX. GEMs were sent
314 for RNA-sequencing to National Genomics Infrastructure of SciLifeLab (Karolinska Institute,
315 Sweden) using the NovaSeq XPlus 25B. Data analysis was performed as the *in vitro* RNAseq
316 dataset, described above. To ensure analysis of human cells, we aligned the libraries to the h38
317 human genome dataset and the m39 mouse genome dataset, and cells with a ratio of
318 human:mouse gene count >1 were processed.

319 **Statistics**

320 The N for the animals was calculated using G-Power 3.1 (Faul et al., 2007) based on prior data
321 from several publications of hemiparkinsonian rodent model behavior (Bjorklund and Dunnett,
322 2019).

323 GraphPad Prism v10.00 was used for generating all graphs and performing statistical analyses.
324 For pairwise comparisons, Student's t-test was utilized. One-way ANOVA or two-way ANOVA
325 with Tukey's or Bonferroni's multiple comparison tests were used to compare multiple
326 variables. Error bars indicate the standard error of the mean (SEM). Significance levels were set
327 as follows: ns = not significant; * = $p<0.05$; ** = $p<0.01$; *** = $p<0.001$; **** = $p<0.0001$.

328

329 **RESULTS**

330 **Longitudinal multiomic single-nuclei sequencing delineates the cell-type composition**
331 **throughout the process of midbrain dopaminergic neuron differentiation in vitro**

332 Building upon our recently published method (Nishimura et al., 2022), we initially designed a
333 new protocol focused on precise midbrain floor plate (mFP) patterning and improving cell
334 viability to generate sufficient progenitor cells, while expanding compatibility to a broader range
335 of human induced pluripotent stem cell lines. We were able to successfully sequentially
336 differentiate iPSC into midbrain progenitor cells, to functional neurons replicating the canonical
337 markers of mDA neurons (Sup. Figure 1).

338 Our primary goal was to investigate the developmental trajectories leading to the generation of
339 mDA neurons *in vitro* from both transcriptomic and epigenomic perspectives. We thus
340 conducted single cell multiomic (ATAC + Gene Expression) sequencing in a wild-type iPSC line,
341 KOLF2.1J, at different developmental stages (Days in vitro (DIV): DIV11, 16, 28, 42 and 56; Figure
342 1A). Following quality control and filtering, we combined manual cell type annotation using
343 cluster-specific marker genes (Clarke et al., 2021; Zhou et al., 2019), with automatic annotation
344 methods (Conde et al., 2022), utilizing reference datasets representing the developing human
345 brain (La Manno et al., 2016). We identified 9,233 high-quality cells, categorized into 8 major
346 types, with sequential differentiation to a mature DA identity (Figure 1B,C). Chronologically,
347 cells from early differentiation phases (DIV11 and 16) exhibited high expression densities of
348 classic markers associated with regional brain identities, such as *LMX1A*, and *OTX2*, reflecting
349 their roles in early neural progenitor stages and initial dopaminergic specification. At DIV28, the
350 expression of *NR4A2* is upregulated; and at advanced phases as DIV42 and 56, markers such as
351 *TH*, *DDC*, and *KCNJ6*, which are associated with mature mDA neuronal identities, displayed high
352 expression densities and chromatin accessibilities, signaling the maturation of dopaminergic
353 neurons (Figure 1F, Sup. Figure 2).

354 We then validated our annotations by comparing them to publicly available scRNA-seq datasets
355 from human fetal midbrain samples (Braun et al., 2023; C. Xu et al., 2023), by quantifying cell
356 type identity across individual cells (Crow et al., 2018). As a result, our annotated cell types
357 closely resembled their endogenous counterparts, as demonstrated by reasonable hierarchical
358 clustering (Figure 1D). High similarity scores (>0.8) were predominantly observed during early
359 stages of the midbrain differentiation and were primarily enriched in precursor cell types such
360 as ProgFP and NbM, underscoring the effectiveness of our approach in recapitulating
361 endogenous early mDA neuron development. Radial glia cell subtypes, Rgl2 and Rgl3, also
362 displayed transcriptomic profiles akin to their counterparts in vivo, hinting at the establishment
363 of an mDA signaling niche to deliver cell type-specific developmental factors for neuronal
364 maturation *in vitro* (Ásgrímsdóttir et al., 2024). At advanced stages, mDA neurons, closely
365 matched their endogenous cells from reference datasets. These findings support the
366 effectiveness and reliability of this protocol in generating desired cell populations, while also
367 implying that additional or prolonged developmental cues may be needed to promote the
368 maturation and survival of postmitotic neurons at later stages.

369 **Reconstructed midbrain dopaminergic neuron differentiation trajectory resolves evolving**
370 **transcriptional profiles throughout lineage specification and maturation**

371 Beyond chronological time, which may not sufficiently capture variations in transcriptomic
372 and/or epigenetic regulation and can be significantly confounded by cellular heterogeneity
373 during differentiation, we sought to delineate the lineage trajectory from neural progenitors to
374 functional neurons using single-cell transcriptional profiles as the roadmap. We isolated and
375 further subcategorized dopaminergic lineage cells (ProgFP, NbM and mDA neurons) from our
376 multimodal dataset and inferred putative dopaminergic trajectories through both transcriptome
377 pseudotime (Cao et al., 2019) and RNA velocity (Bergen et al., 2020). Through calculating the
378 RNA velocity stream and predicted latent time from selected cell types, we discovered that
379 ProgFP and NbM were on a neuronal differentiation path toward mature mDA neurons, aligned
380 with their chronological time (Figure 1G). UMAP-based embeddings of selected cell types
381 revealed that mDA neurons can be arranged in a maturation hierarchy, progressing from the
382 early *Neuron projection* to acquiring the ability for *Neurotransmitter release*, followed by
383 structural maturation through *Synaptic assembly*, and ultimately culminating in functional
384 refinement via *Synaptic modulation*, which aligns with the positioning from the independent
385 pseudotime analysis. Interestingly, a shortcut bypassing the cluster for axonal development on
386 DIV 28 and directly leading to mature mDA neurons, was observed at the advanced
387 differentiation time points (DIV 42 and 56), suggesting that the laminar fate, as an alternative
388 mechanism of neurogenesis and maturation, could be involved in different stages of midbrain
389 cell differentiation (Desai & McConnell, 2000).

390 Furthermore, by employing single-cell regulatory network inference and clustering (SCENIC)
391 methods to analyze active modules of co-regulated genes, we aimed to reinforce our
392 reconstructed developmental trajectories with an additional layer of regulon activity, thereby
393 capturing critical shifts in gene regulatory networks that coincide with transitions in cell
394 identities and functional states (Aibar et al., 2017). Clustering of AUCell scores for activities of
395 each regulon revealed distinct segregation between early neural progenitors, ProgFP, and NbM,
396 and their descendant mDA neurons along the development trajectory (Figure 1H). Regulon
397 similarities were obviously higher among various mDA neuron subcategories, suggesting that
398 mDA lineage specification and maturation are governed by gene networks regulated by a core
399 set of transcription factors, which may undergo slight modifications at different stages of
400 differentiation. Particularly, we observed increased activity of several recognized transcription
401 factors that drive neurogenesis along the mDA lineage. For instance, upregulated NR3C1
402 regulon in ProgFP cells skews neural precursors towards proliferation over differentiation,
403 thereby facilitating the progenitor pool expansion (Nürnberg et al., 2018). SREBF1, a pro-neural
404 transcription factor controlling mDA neurogenesis (Toledo et al., 2020), was identified as one of
405 the most active regulons in ProgFP development, driving its transition to NProg. Similarly,
406 NEUROD1 and NHLH1, neurogenic transcription factors essential for mDA neuron
407 development, were subsequently ranked as the top regulons in NbM, triggering neurogenesis
408 and differentiation in postmitotic cells throughout neural development (W.-Y. Kim, 2012;
409 Murdoch et al., 1999). Subtypes of mDA neurons appeared to share a core set of transcription
410 factors, including PBX1, a classic regulator of mDA specification and survival (Dennis et al.,
411 2019). In contrast, transcription factors as POU2F2 and BCL11A displayed more specialized
412 roles at distinct maturation stages (Tiklová et al., 2019; Tolve et al., 2021). By reconstructing the
413 *in vitro* developmental trajectory, we confirmed that the differentiation protocol successfully
414 replicated mDA neuron embryological development, reflecting similar gene expression

415 dynamics and co-expression regulatory networks. This approach holds potential for the *de novo*
416 identification of developmental regulatory modules, offering deeper insights into dopaminergic
417 neuron differentiation and maturation.

418 **An iterative enhancement in ventralization yields improved floorplate patterning and**
419 **accelerated neuronal conversion in a new protocol**

420 Given that robust regional patterning forms the cornerstone to generate mDA neurons of high
421 quality, and our single-cell datasets suggested that the current cultures could benefit from
422 further ventralization, we aimed to investigate whether enhanced ventralization could improve
423 patterning outcomes, using EN1 as a marker for mDA neuron specification (Simon et al., 2001),
424 and to streamline the protocol to increase scalability and reduce labor intensity.

425 EN1 plays a pivotal role from the earliest stages of regional specification and maintenance of
426 mDA neurons in adulthood (Rekaik et al., 2015). It supports midbrain-hindbrain boundary
427 formation during midbrain development and regulates a critical set of genes (including *TH*,
428 *VMAT2*, *DAT*, and *ALDH1A1*) in postmitotic neurons to sustain mDA function (Albéri et al., 2004;
429 Simon et al., 2001). Thus, EN1 expression serves as a reliable surrogate for enhanced mDA
430 neuron specification and a promising indicator of successful transplantation in vivo (Piao et al.,
431 2021). To replicate an EN1 overexpression, we applied a higher concentration of the SHH
432 agonist purmorphamine (Kriks et al., 2011), and optimized culture conditions to minimize the
433 cytotoxicity, thereby preserving the desired cell viabilities (Figure 2A). Subsequently, increasing
434 concentrations of purmorphamine dramatically boosted EN1 expression, while traditional
435 midbrain floor plate markers, FOXA2 and LMX1A, remained unaffected compared to the original
436 protocol at DIV11 (Figure 2B,E; Sup. Figure 3A,B). By DIV16, during the fate transition from NbM
437 towards early mDA neurons, cell cultures from the new protocol showed a rapid generation of
438 TH^+ neurons, and higher proportion of TH+ cells that co-expressed EN1 and SOX6 (Figure 2C,F),
439 another key transcription factor that is typical of neurons derived from the human SNpc region
440 (Oosterveen et al., 2021). Moreover, in prolonged cell cultures, mDA neurons with enhanced
441 ventralization retained substantial co-expression of EN1 and SOX6 by DIV28 (Figure 2D,G) and
442 exhibited active electrophysiological properties by DIV42 (Figure 2H).

443 We then applied single nuclei sequencing (snRNA-seq) to DIV 14, 16, and 28 cell preparations to
444 assess the quality of iPSC-derived midbrain cells under the new protocol. After filtering, we
445 obtained high-quality 23,534 cells (Figure 3A) and then we integrated transcriptomic profiles
446 from both conditions with Harmony approach (Korsunsky et al., 2019), enabling a comparative
447 analysis by isolating the mDA neuronal lineage from different datasets (Sup. Figure 4B). Under
448 the new protocol, we observed an accelerated differentiation process, with a higher proportion
449 of NProg and NbM emerging at earlier stages, accompanied by a reduction in ProgFP cells
450 (Figure 3B). Using the same annotation methods as in the previous dataset, the resulting mDA
451 lineage cell types were enriched with classic mDA neuron marker genes (Figure 3C), including
452 *FOXA2*, *LMX1A*, *OTX2*, *TH*, *and NR4A2*, and showed an expected developmental trajectory
453 across different cell populations (Figure 3D). In contrast, the new protocol was marked by
454 higher EN1 levels and the sustained expression of OTX2 and SOX6 in postmitotic cells. A
455 transverse comparison of mDA neurons from the new protocol also revealed higher levels of TH,
456 SLC18A2 (VMAT2), and CALB1 (Calbindin 1), suggesting that these cells had preceded further in
457 their maturation (Poulin et al., 2018) (Figure 3F). We then conducted SCENIC analysis to

458 pinpoint key transcription factors activated by the new protocol (Figure 3E). The paired-box
459 transcription factor PAX7 transiently became the dominant regulon in NProg, suggesting precise
460 rostral-caudal patterning as it contributes to determine the midbrain-hindbrain boundary during
461 regionalization (Agoston et al., 2012; Nakamura et al., 2005). Other leading regulons in NProg
462 and NbM cells are also actively involved in guiding the neuronal identity acquisition. For
463 instance, POU3F1 and ZEB1 are essential regulators of neural lineage commitment, often
464 working synergistically to coordinate correct orders of neuronal development, as POU3F1
465 promotes early neural fate decisions, while ZEB1 modulates the developmental timing and
466 prevents premature differentiation (Bella et al., 2021; Gheldof et al., 2011). Notably, PITX3
467 emerged as a leading regulon in mDA neurons, which reflects the progressive acquisition of
468 mature mDA phenotypes (Smidt et al., 2004) and highlights their molecular similarity to
469 endogenous SNpc mDA neurons (Figure 3F,E). Regulon activity profiles from the integrated
470 dataset revealed a distinct and significant regulatory impacts of TCF4 and TCF12 under the new
471 protocol (Sup. Figure 4C). Interestingly, the new protocol also appeared to enhance SREBF1
472 expression throughout differentiation, linking it to its known role in regulating midbrain
473 dopaminergic neurogenesis (Toledo et al., 2020), and its involvement in controlling neuronal
474 dendrite expansion through lipid homeostasis (Ziegler et al., 2017).

475 Overall, the optimization of mDA neuron differentiation protocol resulted in significant
476 advancements in mDA neuron specification and maturation, with higher yield of mDA neurons
477 resembling transcriptomically the ventral subset of human native DA nigral neurons.

478 **Differentiated hiPSC instrastriatal transplant matures into innervated DANs and**
479 **establishes motor recovery in hemiPD mice**

480 After establishing that this protocol produces an enriched ventralized subpopulation *in vitro*, we
481 proceeded to further evaluate these cells *in vivo* using rodent hemiparkinsonian models as
482 proof-of-concept for potential therapeutic approaches and cell differentiation in a more
483 physiological and pathological context. We lesioned unilaterally B6RGS mice by injecting 6-
484 OHDA in the MFB, and once confirmed hemiPD, we randomly selected mice to be injected with
485 200K cells intrastriatally. Motor recovery was assessed continuously by amphetamine-induced
486 ipsilateral rotations, showing that grafted hemiPD animals returned to pre-lesion state 4 months
487 post-implant (m.p.i.), which was maintained 1 month later, ending our grafting experiment
488 (Sham: -0.24 ± 0.73; 6-OHDA: 13.41 ± 1.43; Grafted: -0.70 ±1.18). To ensure overall motor
489 recovery, we also analysed complex motor coordination by tape removal test (Sham: -0.40 ±
490 0.34; 6-OHDA: 19.51 ± 2.50; Grafted: -2.82 ±0.96) and spontaneous motor activity by cylinder
491 wall test (Sham: 51.82 ± 3.73%; 6-OHDA: 8.85 ± 4.75%; Grafted: 40.89 ± 3.73%). Human cells
492 were detected in these 5-month grafts by STEM121^{+} staining, showing that grafted cells did not
493 migrate to other regions (Fig. 4C). Furthermore, human DANs were detected by double positive
494 staining of TH and HuNu, with these cells showing extended prolongations, characteristic of
495 mDA neurons (Fig. 4D, E). Using stereological quantification of TH^{+}/HuNu^{+} cells (Fig. 4F), grafts
496 were estimated to have 160000 human nuclei (155700 ± 35893), of which about 10% were also
497 stained positively for TH (10.36 ± 0.73%). After establishing the presence of DANs within our
498 grafts, we aimed to analyse if these DANs recapitulated the phenotypical aspects of the most
499 PD-vulnerable portion of nigral DANs which have been reported to be A9-subtype (DANs from
500 the SNpc), more specifically the SOX6^{+}/AGTR1a^{+} subpopulation located in the ventral SNpc

501 (Kamath et al., 2022; Salmani et al., 2024). To this aim, we performed a series of IHC analysis of
502 the grafted DANs. A grand majority of grafted TH^+ cells were found to be positive for several
503 markers distinctive to the PD-vulnerable A9-subtype (Fig 4G,H), such as SOX6 (84.67 ± 3.03%),
504 ALDH1A1 (50.67 ± 2.37%) and AGTR1 (64.16 ± 4.97%). In contrast, a minority of the DANS
505 stained positively for the A10-subtype marker Calbindin (29.92 ± 3.45%). Another aspect that we
506 wanted to evaluate is the expression of canonical markers for mDA neurons in the grafted TH^+
507 cells (Fig. 4I,J). We performed IHC and we were able to identify approximately all of the grafted
508 DANs as $LMX1A^+$ (92.09 ± 3.37%), $FOXA2^+$ (96.66 ± 1.88%), $NR4A2^+$ (96.19 ± 2.16%) and $PITX3^+$
509 (85.14 ± 1.80%). Finally, we performed another series of IHC to evaluate expression of proteins
510 involved in DA regulation and secretion (Fig. 4K,L). We were able to determine that the grafted
511 DANs expressed DAT (90.03 ± 1.23%), GIRK2 (96.78 ± 2.12%), VMAT (94.24 ± 1.47%) and DDC
512 (100.00 ± 0.00%). Overall, we were able to demonstrate by IHC that grafted cells mature into a
513 large percentage of DANs expressing canonical markers for A9-subtype mDA neurons that are
514 able to ameliorate motor degeneration in rodent PD models.

515 **snRNA sequencing of grafts identifies a population of A9-subtype mDA neurons *in vivo***

516 One of the several caveats to approach regarding grafted cells is the overall composition of the
517 transplant, as they may contain non-mDA cells that could disturb the putative therapeutic
518 population, and how much do the grafted cells resemble the native human cells. To do so, we
519 proceeded to analyse the transcriptomic profile of snap-frozen endpoint graft tissue punches of
520 3 grafted mice by snRNA-sequencing, and after data quality filtering we obtained 9196 high-
521 quality human nuclei. Grafted differentiated human cells separated into 4 different cluster
522 comprised of neurons, radial glia, gliobasts and oligodendrocyte precursors (Fig. 5A). An in-
523 depth analysis of the neuronal clusters classified into DAergic, Glutamatergic, GABAergic
524 (defined by RBFOX3) and neural progenitors (defined by INA). Interestingly, the DAergic cluster
525 was comprised of 3 subclusters: DA_SOX6, DA_CALB1 and DA_ONECUT2 (Fig. 5B).
526 Furthermore, evaluating the expression levels of genes of interest to each cluster, we were able
527 to identify that each DA subcluster has individually identifiable transcriptomics profile. DA
528 clusters presented high expression levels of genes related to DA cells (*TH, DDC, NR4A2, LMX1A,*
529 *PBX1, SLC18A2* [VMAT2], *SLC6A3* [DAT], *PITX3, KCNJ6* [GIRK2]), while in contrast, GABA cluster
530 and Glut clusters did not, expressing however high levels of *GAD1* and *GAD2*, and *SLC17A6*
531 [VGLUT2] respectively. INA clusters were able to be distinctly separated from Glut clusters by
532 expression levels of *SLC17A6, STMN2 and INA*. Furthermore, DA subclusters can be distinctly
533 separated by differential expression levels of *SOX6*, *CALB1* and *ONECUT2*. (Fig. 5C,D).
534 Approximately half of the cells from the DA subclusters were classified as DA_SOX6 (44.73 ±
535 4.79%), with the other half comprised of a majority of DA_CALB1 and a small proportion of
536 DA_ONECUT2 (Fig. 5E). Our findings show that grafted cells differentiated with this optimized
537 protocol show promising potential to replace $SOX6^+$ specific subtypes of PD-susceptible mDA
538 neurons.

539 **Comparison with pre-established transcriptomic dataset finds similarities between adult**
540 **human midbrain and grafted cells**

541 As we have been able to identify DANs within our human grafted cells, , we wanted to reassure
542 that our hPSCs resembled the expected transcriptomic profile of the human native mDA cells.
543 For such purpose, we performed a MetaNeighbor analysis (Crow et al., 2018) with our DA

544 clusters and DA clusters of the human substantia nigra dataset from Kamath et al. (Kamath et
545 al., 2022) after random downsampling the human dataset to avoid false correlations (Fig 5F).
546 Our analysis showed high distinctive resemblance with a score >0.8 between our DA_SOX6
547 subcluster and the SOX6_AGTR1 subcluster from Kamath dataset, which have been reported to
548 be the most susceptible subpopulation to PD (Kamath et al., 2022; Salmani et al., 2024) . In
549 contrast, the DA_ONECUT2 subcluster showed resemblance to the human CALB1_TRHR
550 reported to be the most resilient. However, the DA_CALB1 subcluster was not able to achieve a
551 distinct resemblance to a specific subpopulation but rather most of the CALB1 human clusters,
552 indicating that these cells are not fully dedicated to a specific subtype and may be prone to
553 further differentiation. This data reinforces that we were successfully able to generate cells that
554 differentiate *in vivo* to cells resembling human SOX6 mDA neurons.

555 **Analysis of gene regulatory networks of interest show that the distinct subpopulations of**
556 **SOX6$^+$ DANs do not shift back to other subtypes**

557 Based on our previous finding about the resemblance of human transcriptomic profile of the DA
558 subcluster, we wanted to evaluate if these cells could potentially lose their distinct identity. We
559 first evaluated the functional transcriptome profile of each cluster based on the GO terms.
560 Based on this analysis, we observed that the DA_SOX6 subcluster is associated with GO terms
561 related to late-stage mature neurons, for example, modulation of synaptic transmission or
562 synapse organization. On contrast, DA_CALB1 is related to GO terms associated with learning,
563 and DA_ONECUT2 with regulation of neuron and cell projection. This indicates that while all
564 subclusters share similar functions as late-stage neurons, each one has their own defining GO
565 clustering. We continued by performing RNA velocity analysis with scVelo (Bergen et al., 2020;
566 Gayoso et al., 2024) on our DA and Immature neurons subclusters and we found that Immature
567 neurons have the potential to become DA_CALB1 cells. Interestingly, the DA_CALB1
568 subclusters have the potential to become either DA_ONECUT2 or DA_SOX6, which in contrast
569 their velocity show that these identities are an endpoint (Fig 5H). Further evaluation of the gene
570 regulatory network by SCENIC establishes that the DA clusters are enriched in exclusive TFs
571 expression profile, not found in the immature neuron, GABA or Glut clusters. For example, PBX1
572 regulon networks have been associated with ventral midbrain DA organization and is highly
573 enriched (score >0.8) in our DA cluster. Moreover, the DA_SOX6 is differentially highly enriched
574 in SOX6 (score >0.8) and CUX2 (score >0.6) within the DA clusters. Interestingly, the CUX2
575 regulon network has been reported to be highly associated with the SOX6$^+$AGTR1$^+$ clusters of
576 neurons in human datasets, further validated in PD macaque models (Kamath et al, 2022; Tang
577 et al., 2023).

578 Overall, as proof-of-concept the combination of the immunohistochemical and transcriptomic
579 data reflects that this new accelerated *in vitro* protocol is able to produce mDA precursors by
580 day 14, which, upon transplantation into a PD model, exhibiting successful motor recovery,
581 selectively differentiate in a majority of PD-susceptible neurons.

582

583 **DISCUSSION**

584 The study presents an enhanced protocol for differentiating midbrain dopaminergic (mDA)
585 neurons from human induced pluripotent stem cells (hiPSCs) based on multiomic

586 transcriptomic analysis of different itterations, highlighting improvements in patterning
587 efficiency and biological reproducibility. This development holds significant promise for PD
588 research, as it addresses key limitations in the previously published differentiation protocol,
589 such as prolonged differentiation timelines, suboptimal ventral patterning, and inconsistent
590 generation of mature mDA neurons across different cell lines.

591 The single nuclei multiomic profiling of differentiated cells at sequential timepoints revealed
592 distinct regulatory networks governing the transition from neural progenitors to mature
593 dopaminergic neurons. By integrating scRNA-seq and scATAC-seq, the study identified
594 temporal shifts in chromatin accessibility and transcriptional activity that mirrored the
595 development of the human midbrain. For instance, the emergence of neurons expressing TH,
596 DDC and KCNJ6 at DIV42 correlated with elevated activity of transcription factors such as PBX1,
597 which is known to play a crucial role in mDA neuron survival and functional maturation.

598 Based on the transcriptomic profiling, it was determined that the current protocol could benefit
599 from the iterative enhancement of the ventralization process, which improved mDA patterning
600 evidenced by elevated EN1 expression (a key marker for mDA neuron specification). This
601 adjustment was particularly beneficial in producing neurons that more closely resemble the
602 human SNpc dopaminergic neurons, the primary neuronal population affected in Parkinson's
603 disease. Furthermore, we were able to identify regulatory networks involving mDA neuron
604 maturation enriched in the new protocol, such as TCF12 and TCF4. Specifically, TCF12 plays a
605 dual role in the early commitment of neural progenitors and the late specification of neuronal
606 subsets, with its loss leading to altered expression of TH and AHD2 (ALDH1A1), the latter being
607 crucial for the specification and maintenance of dopaminergic neurons, particularly in the A9
608 dopaminergic neuronal group (Chung et al., 2005). TCF4, on the other hand, is likely involved in
609 the fine-tuning of neuron identity during the onset of mDA neuron subtype specification. In a
610 mouse study, deletion of TCF4 led to delayed maturation of dopaminergic neurons, primarily
611 through transient suppression of *Ahd2* and *Nxph3* (Mesman et al., 2021).

612 One of the critical advancements was the precise modulation of the midbrain floor plate (mFP)
613 patterning using optimized coating conditions (LN511) and biphasic activation of WNT signaling
614 (CHIR boost), which resulted in a substantial population of mFP progenitors by day 11 of
615 differentiation and improved the expression of essential mDA markers such as FOXA2, LMX1A,
616 and OTX2. This suggests that the updated protocol not only enhances patterning but also
617 reduces contamination by non-neural cell types, a persistent issue in generating region-specific
618 neurons for disease modelling. Notably, the cellular composition differed from that generated
619 using the original protocol due to enhanced patterning efficacies of floorplate progenitors, and
620 the removal of the MEK/ERK pathway inhibitor PD0325901 and the FGF receptor inhibitor
621 SU5402, that mainly used to repress expansion of SOX2+ radial glia and progenitor cells (Koch
622 et al., 2009).

623 Despite the absence of pro-neural effects from PD0325901 and SU5402 in the new protocol, our
624 cell cultures still produced a greater number of mDA neurons with more mature morphological
625 and molecular phenotypes, particularly in terms of synapse assembly, relying solely on intrinsic
626 mechanisms. Moreover, the integration of synthetic LXR ligands (GW3965) further accelerated
627 neurogenesis process, leading to the earlier emergence of mature dopaminergic neurons.
628 Specifically, TH^+ neurons first appeared at day 16, notably earlier than in previously published

protocols, where they typically emerged around day 21. The early establishment of mDA neurons facilitates downstream functional assays, such as live-cell calcium recordings and neurotransmitter release analysis, thus shortening the experimental timeline and allowing for earlier detection of phenotypic differences.

Subsequent electrophysiological analysis via live-cell calcium recordings demonstrated that mDA neurons derived using this protocol manifested hallmarks of functionally active neurons, such as spontaneous electrical activity and robust responses to depolarization stimuli (Chan et al., 2007; Pissadaki and Bolam, 2013) . These findings are significant, as they confirm that the cells generated are not merely phenotypically similar to mDA neurons but also functionally active, which is critical for accurate disease modeling and therapeutic screening.

The study successfully achieved scalable and reproducible mDA neuron differentiation across multiple iPSC lines, including those derived from Parkinsonian patients, suggesting that this protocol can serve as a standardized approach for large-scale production of high-quality dopaminergic neurons. Such advancements are pivotal for the development of robust in vitro models to study neurodegenerative diseases and for testing potential therapeutic interventions.

Finally, as proof-of concept validation for therapeutic approaches, we were able to determine that the new protocol could produce mFP progenitors and NbM able to differentiate *in vivo* to mDA neurons resembling the A9-subtype nigral neurons in majority, based on expression of proteins such as SOX6, AGTR1, GIRK2 or ALDH1A, reported to be more susceptible to PD in human and animal models (Kamath et al., 2022, del Rey et al.,2024, Nie et al., 2024, Salmani et al., 2024). Furthermore, evaluation of the transcriptomic profile of the DA neurons in the graft showed high resemblance to the human counterpart, specially the SOX6-AGTR1A mDA neurons. This proposes that these cells could have great potential for directed replacement therapies.

While these advancements could be of great interest to the PD research community, we have to address several caveats. First, we only have established the replicability of this protocol on hIPSC, both WT and with GBA mutations. But further characterization with more well known mutations found in familial PD, such as GBA E326K, LRRK2 G2019S or the triplicate SNCA, could elucidate the validity of this enhanced protocol. Furthermore, the use of human embryonic stem cells has not been proposed for this study. More *in vitro* studies would be of interest to validate further this new protocol. Another caveat to address is the pre-clinical aspect, as the *in vivo* experiments were only used as proof-of-concept for therapeutical approaches. Further grafting experiments with PD-mutated hiPSC cell lines and a more in-depth preclinical analysis could detail if this protocol would be a much better advantage that the current available protocols, which so far have shown to be safe in clinical trials (Sawamoto et al., 2025, Tabar et al;, 2025). Moreover, the longevity of the grafting experiment was decided upon stable motor recovery, so we do not have an overview of the long-term effects of these grafts, whether other contaminants can appear or tumorigenesis in aged individuals.

CONCLUSIONS

In conclusion, the optimized differentiation protocol represents a significant step forward for stem cell-based approaches in modeling PD and for future applications in regenerative medicine. By boosting the timed expression of EN1, we have achieved a more efficient and consistent generation of mDA neurons, with mature phenotypes targeting the A9 subtype defined mainly by the expression of SOX6, ALDH1A, GIRK2 and AGTR1. The study sets the stage for more accurate disease modeling and lays the groundwork for potential directed cell replacement strategies.

ACKNOWLEDGMENTS

RGS., GL and EA conceptualized the experiments. RGS and GL redacted the manuscript. RGS performed *in vivo* experiments; GL, RK, CS, CT and AX contributed to the *in vitro* protocol development. JCK contributed to the calcium imaging analysis. GL and AX contributed to the *in vitro* transcriptional analysis; RGS and CA performed the graft nuclei isolation, and GL the transcriptional analysis. CS, GCB and OD reviewed the manuscript.

This work was mainly supported by the European Union's Horizon 2020 (H2020) Research and Innovation Programme (Neurostemcell-Reconstruct 874758/EA) and the European Research Council (ERC) PreciseCellPD grant (Grant No. 884608/EA). Other contributors: Knut and Alice Wallenberg Foundation Wallenberg Scholar 2018.0232/EA, Vetenskaprådet VR2020-01426/EA, Chan Zuckerberg Initiative and the Silicon Valley Community Foundation (2018-191929)/EA, H2020 MSCA-ITN ASCTN/EA, H2020 Grant No. 899687 - HS-SEQ, Aligning Science Across Parkinson's (ASAP-20505)/EA, Hjärnfonden project FO2024-0195/EA. JCK and PU were supported by the German Science Foundation (516641042) and the Wenner-Gren foundation (UPD2022-0159) respectively.

The authors acknowledge support from the National Genomics Infrastructure in Stockholm funded by Science for Life Laboratory, the Knut and Alice Wallenberg Foundation and the Swedish Research Council, and NAISS/Uppsala Multidisciplinary Center for Advanced Computational Science for assistance with massively parallel sequencing and access to the UPPMAX computational infrastructure. We are really thankful for the help of the Molecular Neurobiology unit of the Medical Biochemistry and Biophysics of the Karolinska Institute, especially Gonçalo Castelo-Branco and Onur Dagliyan for their input. We posthumously want to thank Prof. Ernest Arenas, whom without this project could not have been possible.

FIGURES

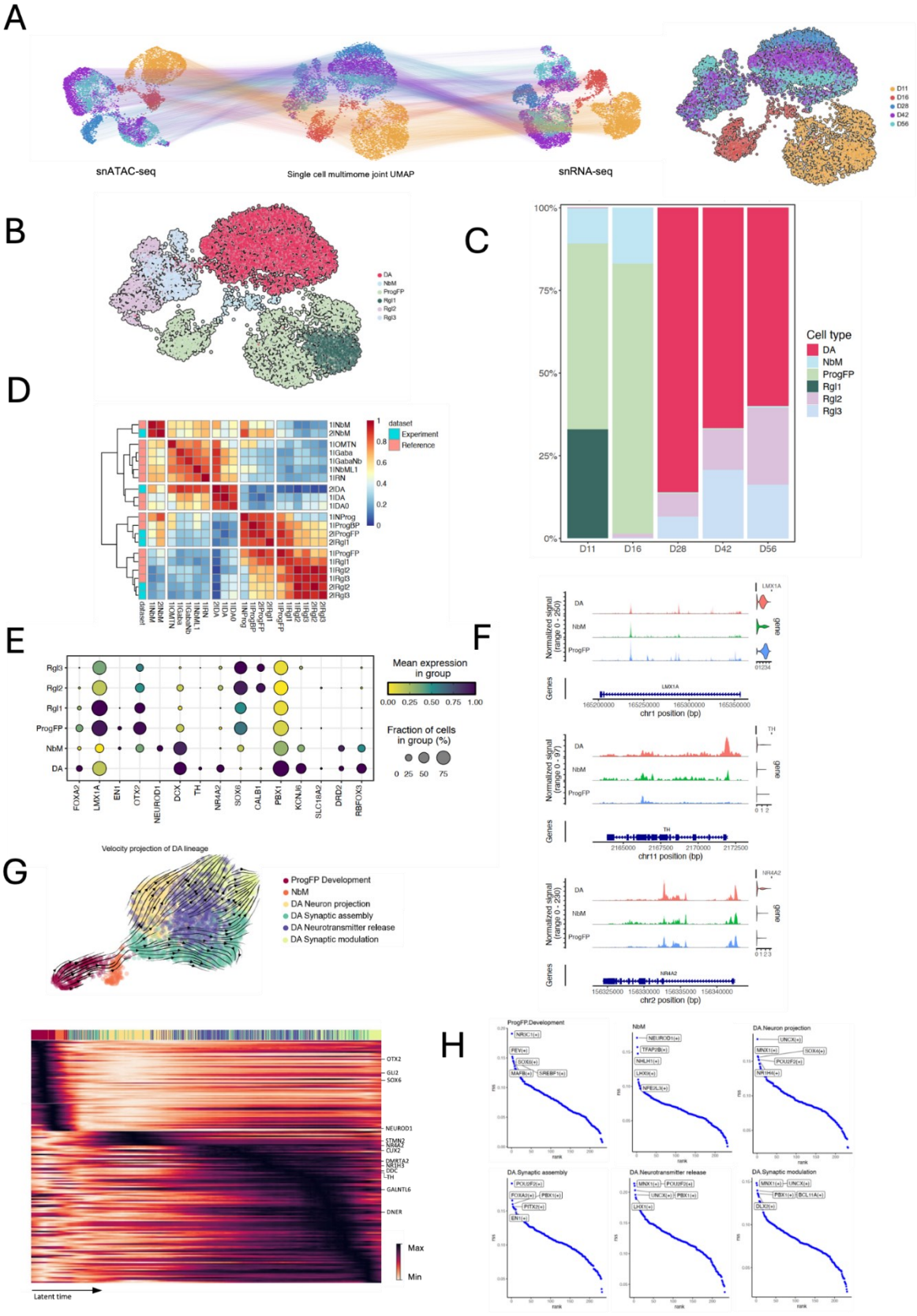

Figure 1. Multiomic single-nuclei RNA sequencing revealed the diversity of cellular composition throughout of mDA neuron differentiation *in vitro*. (A) Uniform manifold

706 approximation and projection (UMAP) of time-course cell preparations profiled with
707 simultaneous snRNA-seq and snATAC-seq, along with their derivative joint UMAP embedding
708 showing clustering of cells based on both transcriptomic and chromatin accessibility profiles,
709 colored by different time points from DIV 11 to 56. (B) Annotated bimodal UMAP embedding of
710 mDA differentiation in vitro using KOLF2.1J iPSCs. Cell types were manually annotated with top-
711 ranked marker genes and their enriched GO terms. (C) Proportion of cells belonging to each cell
712 type at each differentiation time point. (D) A heatmap of AUROC scores comparing annotated
713 cell types derived from *in vitro* differentiation in this study with those from a publicly available
714 first-trimester human midbrain dataset. (E) A dot plot visualizing the expression levels and the
715 percentage of cells expressing curated key genes across cell types during mDA neuron
716 differentiation. (F) Normalized chromatin accessibility tracks of representative marker genes
717 (LMX1A, TH and NR4A2) of dopaminergic lineage cell types. (G) UMAP embeddings showing RNA
718 velocity projection in mDA-related cell types, and a heatmap displaying gene expression
719 dynamics of cluster driver genes ordered by their inferred latent time. (H) Regulon specificity
720 score (RSS) plots highlighting the top 5 cell type-specific transcription factors involved in mDA
721 differentiation.

722

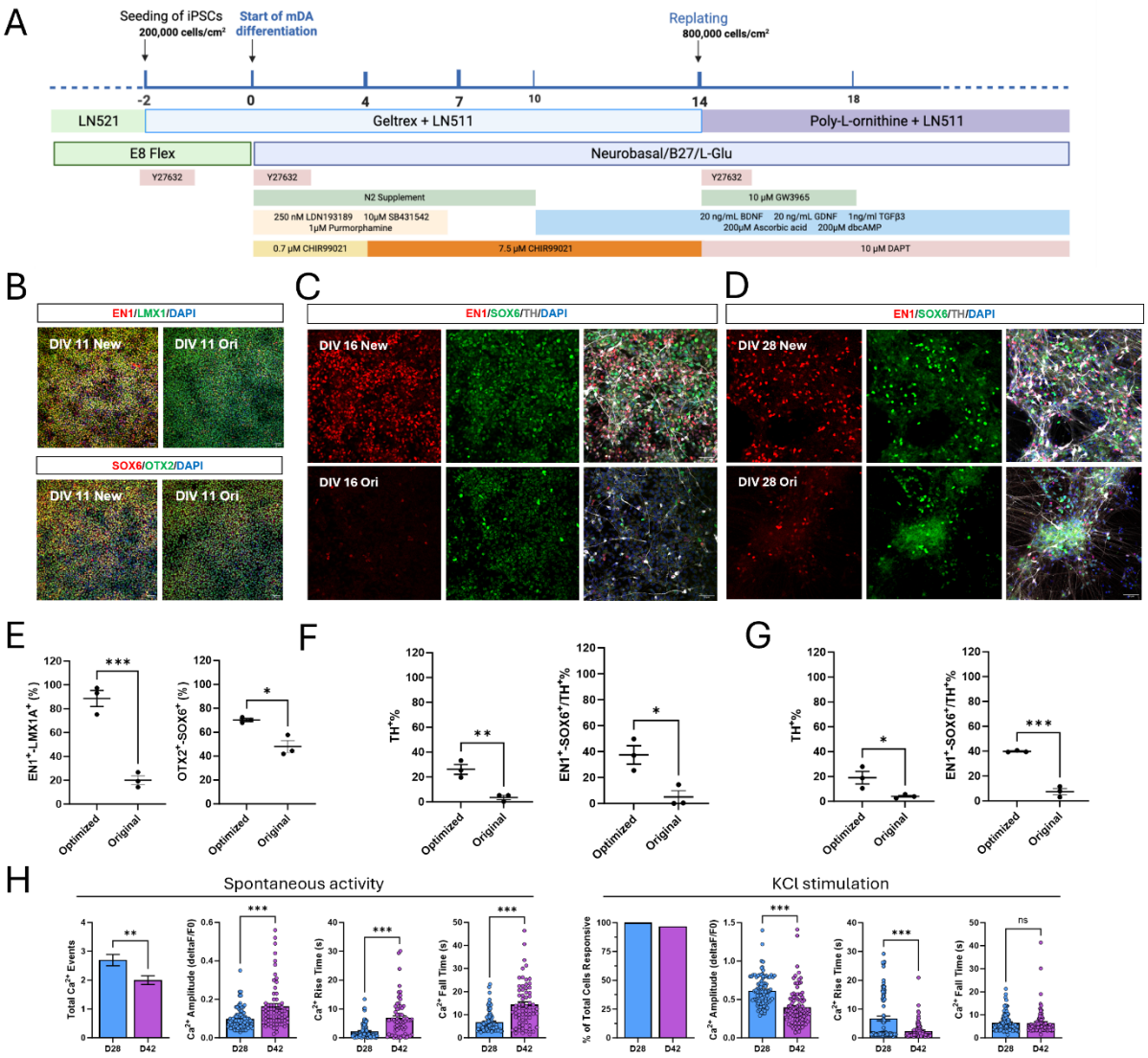

Figure 2. Prolonged ventralization promotes accelerated differentiation of mDA neurons. (A) Schematic depiction of the protocol for differentiating mDA neurons, illustrating the application of pharmacological compounds and growth factors. Representative immunocytochemical images and quantification from both original protocol and new protocol showing (B, E) efficacies of midbrain floorplate patterning at DIV11, showing co-localizations of LMX1+/EN1+ and SOX6+/OTX2+; and EN1+/SOX6+/TH+ neurons at DIV 16 (C, F) and 28 (D, G). White scale bars = 50, 100 μm as indicated (n = 3 independent experiments, error bars are SEM, ns = not significant; * = p<0.05; ** = p<0.01; *** = p<0.001; **** = p<0.0001). (H) Calcium imaging recordings of spontaneous and KCl-induced activities on DIV 28 and 42, presenting the total number of calcium events per neuron recorded, and the percentages of cells responding to KCl-induced depolarization. Metrics of activities, including amplitude, rise time, and fall time of calcium signals, are depicted in the subsequent bar plots.

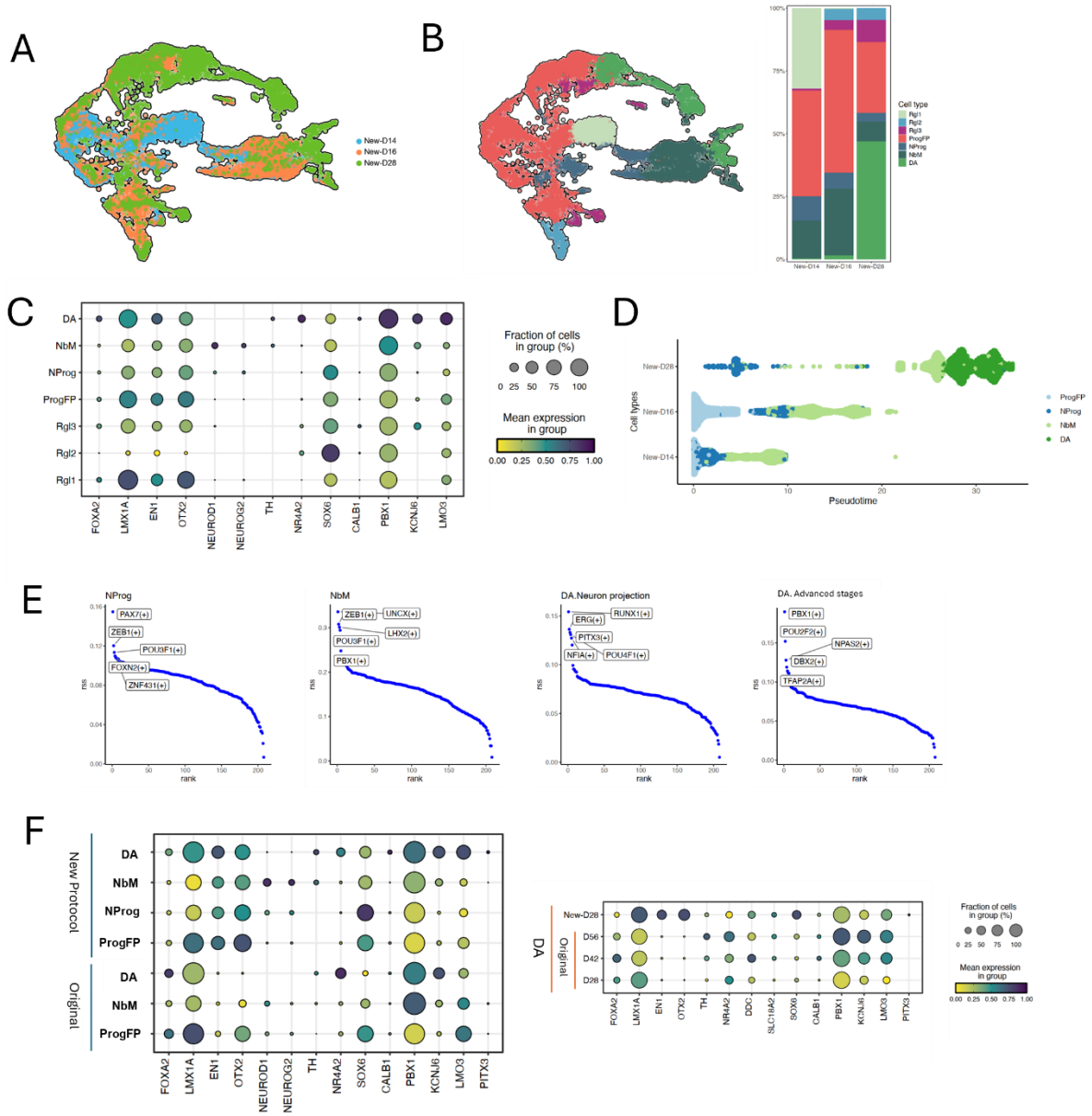

Figure 3. Cell preparations under the new protocol suggested improved molecular phenotypes during *in vitro* midbrain differentiation. (A) UMAP embeddings of mDA differentiation in vitro using KOLF2.1J iPSCs under the new protocol, color coded by different time points at DIV 14, 16 and 28. (B) UMAP embeddings of detailed cell types were manually annotated using top-ranked marker genes and their enriched GO terms, and proportion of cells classified into each cell type per differentiation time point. (C) Dot plot visualizing the expression levels and the percentage of cells expressing curated key genes across distinct cell types generated under the new protocol. (D) Pseudotime trajectory analysis showing progression from progenitor-like populations (ProgFP, NProg, and NbM) to differentiated DA neurons. Cells are ordered by inferred pseudotime along the x-axis. (E) Regulon specificity score (RSS) plots highlighting the top 5 cell type-specific transcription factors driving mDA differentiation under the new protocol. (F) Dot plots showing the expression levels and the percentage of cells expressing midbrain dopaminergic lineage marker genes after integration in (left) midbrain cells categorized as dopaminergic neurons (DA) (right), dopaminergic lineage cell types across all timepoints and both conditions.

754

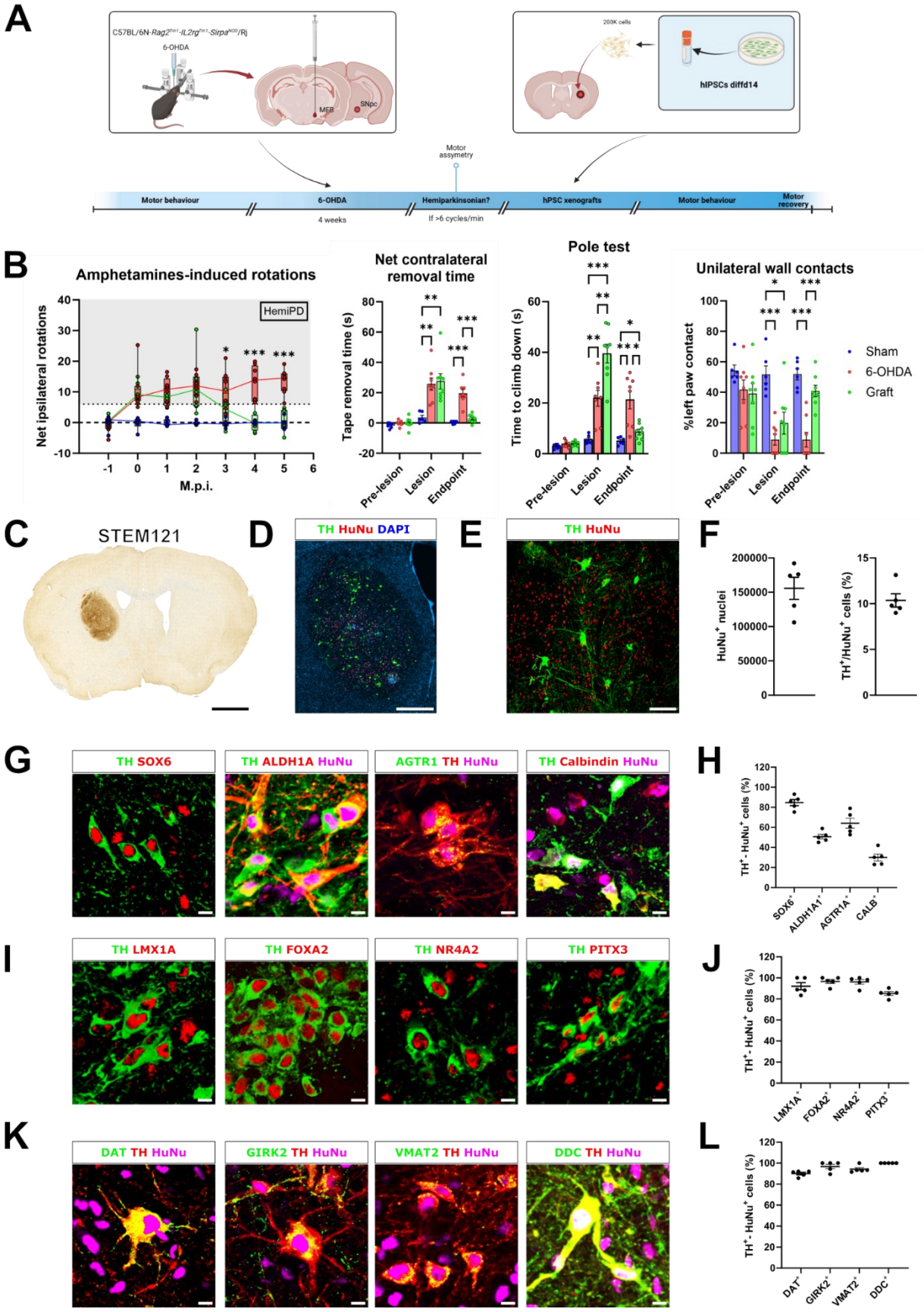
A
C57BL/6N-Rag2tm1-IL2rgtm1-Sirpa NOD/Rj
6-OHDA
MFB
SNpc
200K cells
hIPSCs diffd14
Motor assymetry
Motor behaviour
6-OHDA
4 weeks
Hemiparkinsonian?
If >6 cycles/min
hPSC xenografts
Motor behaviour
Motor recovery
B
Amphetamines-induced rotations
HemiPD
Net ipsilateral rotations
M.p.i.
Net contralateral removal time
Tape removal time (s)
Pole test
Time to climb down (s)
Unilateral wall contacts
%left paw contact
Pre-lesion
Lesion
Endpoint
Sham
6-OHDA
Graft
C
STEM121
D
TH HuNu DAPI
E
TH HuNu
F
HuNu+ nuclei
TH+/HuNu+ cells (%)
G
TH SOX6
TH ALDH1A HuNu
AGTR1 TH HuNu
TH Calbindin HuNu
H
TH+- HuNu+ cells (%)
SOX6+
ALDH1A1+
AGTR1+
CALB+
I
TH LMX1A
TH FOXA2
TH NR4A2
TH PITX3
J
TH+- HuNu+ cells (%)
LMX1A+
FOXA2+
NR4A2+
PITX3+
K
DAT TH HuNu
GIRK2 TH HuNu
VMAT2 TH HuNu
DDC TH HuNu
L
TH+- HuNu+ cells (%)
DAT+
GIRK2+
VMAT2+
DDC+

755

Figure 4. Transplantation of hiPSC differentiated with new protocol. (A) Diagram of the experimental design for the implantation of day 14-differentiated hiPSC in B6RGS mice. (B) Motor recovery is observed by continuous analysis of amphetamine-induced ipsilateral rotation (left), endpoint tape removal test (middle) and endpoint cylinder wall analysis (right). Of note, grafted animals recover pre-lesion state while the 6-OHDA control animals maintain the lesioned state. (C) Example of grafted tissue, stained against STEM121, showing the human cells within the graft. (D) Micrograph of graft stained against TH and HuNu, showing hDANs all over the graft. (E) Closeup of grafted hDANs showing elongated and ramified extensions. (F) Stereological estimate of $HuNu^+$ nuclei (left) and percentage of hDANs (TH^+-$HuNu^+$) in grafts (right). (G) Representative examples of hDANs stained positive for A9-subtype marker, SOX6, ALDH1A1, AGTR1A and A10 marker, Calbindin. (H) Quantification of percentage of hDANs (TH^+-$HuNu^+$) expressing SOX6, ALDH1A1, AGTR1A and Calbindin. (I) Representative examples of hDANs stained positive for mDA neuron makers, LMX1A, FOXA2, NR4A2 and PITX3. (J) Quantification of percentage of hDANs (TH^+-$HuNu^+$) expressing LMX1A, FOXA2, NR4A2 and PITX3. (K) Representative examples of hDANs stained positive for proteins involved in DA excretion, DAT, GIRK2, VMAT2 and DDC. (L) Quantification of percentage of hDANs (TH^+-$HuNu^+$) expressing DAT, GIRK2, VMAT2 and DDC. m.p.i = months post-implant. N for animal behavioral experiment = sham: 6; 6-OHDA: 8; hIPSC-grafted: 8. N for IHC = 5. Scale bar = C: 1mm; D: 500 µm; E: 100 µm; G,I,K: 10 µm.

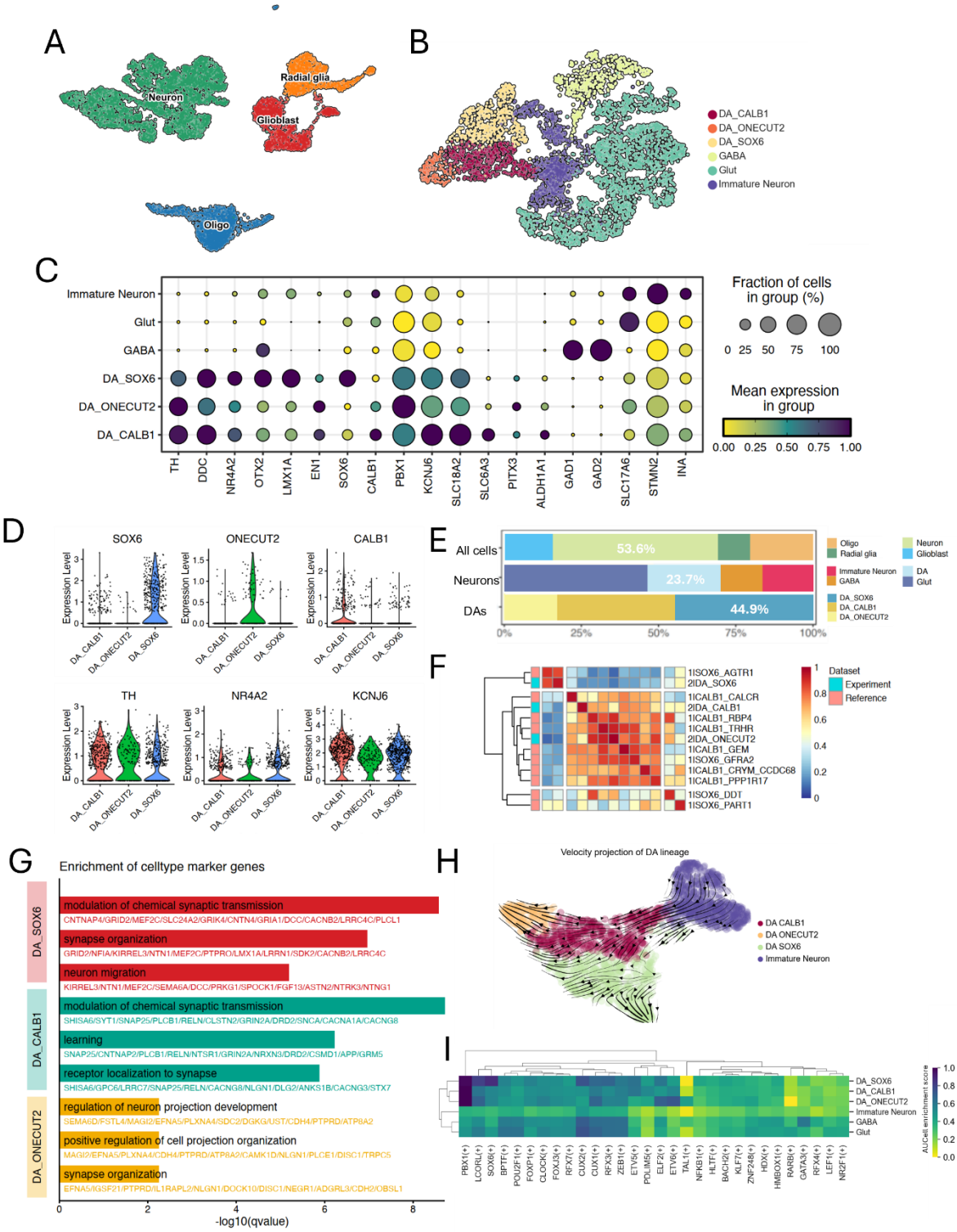

Figure 5. An in-depth single nucleus RNA sequencing characterization of *in vivo* xenograft cellular composition. Annotated UMAP embeddings of (A) 9,196 high-quality human nuclei recovered from three grafted mice at five months post-transplantation, with cells classified into neurons, radial glia, gliobasts and oligodendrocyte precursors; and (B) neuronal population was consisted of immature neurons, GABAergic neurons, Glutamatergic neurons and 3 subtypes of mDA neurons, each characterized by specific transcription factors, as DA_CALB1, DA_ONECUT2, and DA_SOX6. (C) Dot plot showing average gene expression and percentage of expressing cells for selected marker genes across annotated neuronal cell types. (D) Violin plots

785 of representative marker genes for dopaminergic subtypes (SOX6, ONECUT2, CALB1), pan-DA
786 markers (TH, NR4A2, KCNJ6), illustrating subtype-specific and shared expression patterns. (E)
787 Average proportion of yielded human nuclei in each cellular hierarchy across three individual
788 datasets, demonstrating consistent representation of DA subtypes (N=3). (F) MetaNeighbor
789 analysis between transplanted mDA neurons in this study and a reference dataset of DA
790 neurons from the SNpc region of PD patients and matched controls, suggesting transcriptional
791 similarities between DA_SOX6 subtype and SOX6_AGTR1 subtype from the reference dataset.
792 (G) Gene Ontology (GO) enrichment analysis of DA subtype-specific markers, showing distinct
793 biological processes enriched in DA_SOX6, DA_CALB1, and DA_ONECUT2 populations. (H) RNA
794 velocity projection of mDA neuron trajectories in UMAP embeddings, suggesting differentiation
795 pathways among different DA subtypes and immature neurons. (I) Heatmap of average regulon
796 activities of the top 30 transcription factors across mDA and other neuronal subtypes.

797

798 **BIBLIOGRAPHY**

799 Agoston, Z., Li, N., Haslinger, A., Wizenmann, A., & Schulte, D. (2012). Genetic and physical
800 interaction of Meis2, Pax3 and Pax7 during dorsal midbrain development. *BMC*
801 *Developmental Biology*, *12*(1), 10. https://doi.org/10.1186/1471-213X-12-10

802 Aibar, S., González-Blas, C. B., Moerman, T., Huynh-Thu, V. A., Imrichova, H., Hulselmans, G.,
803 Rambow, F., Marine, J. C., Geurts, P., Aerts, J., Van Den Oord, J., Atak, Z. K., Wouters, J., &
804 Aerts, S. (2017). SCENIC: Single-cell regulatory network inference and clustering. *Nature*
805 *Methods*, *14*(11), 1083–1086. https://doi.org/10.1038/NMETH.4463

806 Albéri, L., Sgadò, P., & Simon, H. H. (2004). Engrailed genes are cell-autonomously required to
807 prevent apoptosis in mesencephalic dopaminergic neurons. *Development*, *131*(13), 3229–
808 3236. https://doi.org/10.1242/DEV.01128

809 Alquicira-Hernandez, J., & Powell, J. E. (2021). Nebulosa recovers single-cell gene expression
810 signals by kernel density estimation. *Bioinformatics*, *37*(16), 2485–2487.
811 https://doi.org/10.1093/bioinformatics/btab003

812 Andersson, E., Jensen, J. B., Parmar, M., Guillemot, F., & Björklund, A. (2006). Development of
813 the mesencephalic dopaminergic neuron system is compromised in the absence of
814 neurogenin 2. *Development*, *133*(3), 507–516. https://doi.org/10.1242/dev.02224

815 Bankhead, P., Loughrey, M. B., Fernández, J. A., Dombrowski, Y., McArt, D. G., Dunne, P. D.,
816 McQuaid, S., Gray, R. T., Murray, L. J., Coleman, H. G., James, J. A., Salto-Tellez, M., &
817 Hamilton, P. W. (2017). QuPath: Open source software for digital pathology image analysis.
818 *Scientific Reports 2017 7:1*, *7*(1), 1–7. https://doi.org/10.1038/s41598-017-17204-5

819 Bergen, V., Lange, M., Peidli, S., Wolf, F. A., & Theis, F. J. (2020). Generalizing RNA velocity to
820 transient cell states through dynamical modeling. *Nature Biotechnology 2020 38:12*,
821 *38*(12), 1408–1414. https://doi.org/10.1038/s41587-020-0591-3

822 Björklund, A., & Dunnett, S. B. (2019). The Amphetamine Induced Rotation Test: A Re-
823 Assessment of Its Use as a Tool to Monitor Motor Impairment and Functional Recovery in
824 Rodent Models of Parkinson's Disease. *Journal of Parkinson's Disease*, *9*(1), 17–29.
825 https://doi.org/10.3233/JPD-181525

Björklund, A., & Parmar, M. (2021). Dopamine Cell Therapy: From Cell Replacement to Circuitry Repair. *Journal of Parkinson's Disease*, *11*(Suppl 2), S159. https://doi.org/10.3233/JPD-212609

Bodea, G. O., Spille, J.-H., Abe, P., Andersson, A. S., Acker-Palmer, A., Stumm, R., Kubitscheck, U., & Blaess, S. (2014). Reelin and CXCL12 regulate distinct migratory behaviors during the development of the dopaminergic system. *Development*, *141*(3), 661–673. https://doi.org/10.1242/dev.099937

Braun, E., Danan-Gotthold, M., Borm, L. E., Lee, K. W., Vinsland, E., Lönnerberg, P., Hu, L., Li, X., He, X., Andrusivová, Ž., Lundeberg, J., Barker, R. A., Arenas, E., Sundström, E., & Linnarsson, S. (2023). Comprehensive cell atlas of the first-trimester developing human brain. *Science (New York, N.Y.)*, *382*(6667), eadf1226. https://doi.org/10.1126/science.adf1226

Brichta, L., Greengard, P., & Flajolet, M. (2013). Advances in the pharmacological treatment of Parkinson's disease: targeting neurotransmitter systems. *Trends in Neurosciences*, *36*(9), 543–554. https://doi.org/10.1016/j.tins.2013.06.003

Cao, J., Spielmann, M., Qiu, X., Huang, X., Ibrahim, D. M., Hill, A. J., Zhang, F., Mundlos, S., Christiansen, L., Steemers, F. J., Trapnell, C., & Shendure, J. (2019). The single-cell transcriptional landscape of mammalian organogenesis. *Nature 2019 566:7745*, *566*(7745), 496–502. https://doi.org/10.1038/s41586-019-0969-xr

Chan, C. S., Guzman, J. N., Ilijic, E., Mercer, J. N., Rick, C., Tkatch, T., Meredith, G. E., & Surmeier, D. J. (2007). "Rejuvenation" protects neurons in mouse models of Parkinson's disease. *Nature*, *447*(7148), 1081–1086. https://doi.org/10.1038/NATURE05865

Chung, S., Hedlund, E., Hwang, M., Kim, D. W., Shin, B. S., Hwang, D. Y., Kang, U. J., Isacson, O., & Kim, K. S. (2005). The homeodomain transcription factor Pitx3 facilitates differentiation of mouse embryonic stem cells into AHD2-expressing dopaminergic neurons. *Molecular and Cellular Neuroscience*, *28*(2), 241–252. https://doi.org/10.1016/J.MCN.2004.09.008

Clarke, Z. A., Andrews, T. S., Atif, J., Pouyabahar, D., Innes, B. T., MacParland, S. A., & Bader, G. D. (2021). Tutorial: guidelines for annotating single-cell transcriptomic maps using automated and manual methods. *Nature Protocols 2021 16:6*, *16*(6), 2749–2764. https://doi.org/10.1038/s41596-021-00534-0

Crow, M., Paul, A., Ballouz, S., Huang, Z. J., & Gillis, J. (2018). Characterizing the replicability of cell types defined by single cell RNA-sequencing data using MetaNeighbor. *Nature Communications 2018 9:1*, *9*(1), 1–12. https://doi.org/10.1038/s41467-018-03282-0

Damier, P., Hirsch, E. C., Agid, Y., & Graybiel, A. M. (1999). The substantia nigra of the human brain: II. Patterns of loss of dopamine-containing neurons in Parkinson's disease. *Brain*, *122*(8), 1437–1448. https://doi.org/10.1093/BRAIN/122.8.1437

del Rey, N. L. G., Hernández-Pinedo, N., Carrillo, M., del Cerro, M., Esteban-García, N., Trigo-Damas, I., Monje, M. H. G., Lanciego, J. L., Cavada, C., Obeso, J. A., & Blesa, J. (2024). Calbindin and Girk2/Aldh1a1 define resilient vs vulnerable dopaminergic neurons in a primate Parkinson's disease model. *Npj Parkinson's Disease 2024 10:1*, *10*(1), 1–15. https://doi.org/10.1038/s41531-024-00777-0

867 Dennis, D. J., Han, S., & Schuurmans, C. (2019). bHLH transcription factors in neural
868 development, disease, and reprogramming. *Brain Research*, *1705*, 48–65.
869 https://doi.org/10.1016/J.BRAINRES.2018.03.013

870 Desai, A. R., & McConnell, S. K. (2000). Progressive restriction in fate potential by neural
871 progenitors during cerebral cortical development. *Development*, *127*(13), 2863–2872.
872 https://doi.org/10.1242/DEV.127.13.2863

873 Di Bella, D. J., Habibi, E., Stickels, R. R., Scalia, G., Brown, J., Yadollahpour, P., Yang, S. M.,
874 Abbate, C., Biancalani, T., Macosko, E. Z., Chen, F., Regev, A., & Arlotta, P. (2021).
875 Molecular logic of cellular diversification in the mouse cerebral cortex. *Nature 2021*
876 *595:7868*, *595*(7868), 554–559. https://doi.org/10.1038/s41586-021-03670-5

877 Doi, D., Samata, B., Katsukawa, M., Kikuchi, T., Morizane, A., Ono, Y., Sekiguchi, K., Nakagawa,
878 M., Parmar, M., & Takahashi, J. (2014). Isolation of human induced pluripotent stem cell-
879 derived dopaminergic progenitors by cell sorting for successful transplantation. *Stem Cell*
880 *Reports*, *2*(3), 337–350. https://doi.org/10.1016/j.stemcr.2014.01.013

881 Domínguez Conde, C., Xu, C., Jarvis, L. B., Rainbow, D. B., Wells, S. B., Gomes, T., Howlett, S. K.,
882 Suchanek, O., Polanski, K., King, H. W., Mamanova, L., Huang, N., Szabo, P. A., Richardson,
883 L., Bolt, L., Fasouli, E. S., Mahbubani, K. T., Prete, M., Tuck, L., ... Teichmann, S. A. (2022).
884 Cross-tissue immune cell analysis reveals tissue-specific features in humans. *Science*
885 *(New York, N.Y.)*, *376*(6594), eabl5197. https://doi.org/10.1126/science.abl5197

886 Faul, F., Erdfelder, E., Lang, A. G., & Buchner, A. (2007). G*Power 3: a flexible statistical power
887 analysis program for the social, behavioral, and biomedical sciences. *Behavior Research*
888 *Methods*, *39*(2), 175–191. https://doi.org/10.3758/BF03193146

889 Ferri, A. L. M., Lin, W., Mavromatakis, Y. E., Wang, J. C., Sasaki, H., Whitsett, J. A., & Ang, S. L.
890 (2007). Foxa1 and Foxa2 regulate multiple phases of midbrain dopaminergic neuron
891 development in a dosage-dependent manner. *Development*, *134*(15), 2761–2769.
892 https://doi.org/10.1242/DEV.000141

893 Garritsen, O., van Battum, E. Y., Grossouw, L. M., & Pasterkamp, R. J. (2023). Development,
894 wiring and function of dopamine neuron subtypes. *Nature Reviews Neuroscience*, *24*(3),
895 134–152. https://doi.org/10.1038/s41583-022-00669-3

896 Gayoso, A., Weiler, P., Lotfollahi, M., Klein, D., Hong, J., Streets, A., Theis, F. J., & Yosef, N.
897 (2023). Deep generative modeling of transcriptional dynamics for RNA velocity analysis in
898 single cells. *Nature Methods 2023 21:1*, *21*(1), 50–59. https://doi.org/10.1038/s41592-023-
899 01994-w

900 Gheldof, A., Hulpiau, P., van Roy, F., De Craene, B., & Berx, G. (2012). Evolutionary functional
901 analysis and molecular regulation of the ZEB transcription factors. *Cellular and Molecular*
902 *Life Sciences : CMLS*, *69*(15), 2527–2541. https://doi.org/10.1007/s00018-012-0935-3

903 Gleeson, J. G., Lin, P. T., Flanagan, L. A., & Walsh, C. A. (1999). Doublecortin is a microtubule-
904 associated protein and is expressed widely by migrating neurons. *Neuron*, *23*(2), 257–271.
905 https://doi.org/10.1016/s0896-6273(00)80778-3

906 Greene, P. E., Fahn, S., Eidelberg, D., Bjugstad, K. B., Breeze, R. E., & Freed, C. R. (2021).
907 Persistent dyskinesias in patients with fetal tissue transplantation for Parkinson disease.
908 NPJ Parkinson's Disease, 7(1). https://doi.org/10.1038/S41531-021-00183-W

Jiang, Y. Q., & Oblinger, M. M. (1992). Differential regulation of βiii and other tubulin genes during peripheral and central neuron development. *Journal of Cell Science*, *103*(3), 643–651. https://doi.org/10.1242/JCS.103.3.643

Kamath, T., Abdulraouf, A., Burris, S. J., Langlieb, J., Gazestani, V., Nadaf, N. M., Balderrama, K., Vanderburg, C., & Macosko, E. Z. (2022). Single-cell genomic profiling of human dopamine neurons identifies a population that selectively degenerates in Parkinson's disease. *Nature Neuroscience 2022 25:5*, *25*(5), 588–595. https://doi.org/10.1038/s41593-022-01061-1

Kawamoto, E. M., Vivar, C., & Camandola, S. (2012). Physiology and Pathology of Calcium Signaling in the Brain. *Frontiers in Pharmacology*, *3*, 22359. https://doi.org/10.3389/fphar.2012.00061

Kele, J., Simplicio, N., Ferri, A. L. M., Mira, H., Guillemot, F., Arenas, E., & Ang, S. L. (2006). Neurogenin 2 is required for the development of ventral midbrain dopaminergic neurons. *Development*, *133*(3), 495–505. https://doi.org/10.1242/DEV.02223

Kim, T. W., Piao, J., Koo, S. Y., Kriks, S., Chung, S. Y., Betel, D., Socci, N. D., Choi, S. J., Zabierowski, S., Dubose, B. N., Hill, E. J., Mosharov, E. V., Irion, S., Tomishima, M. J., Tabar, V., & Studer, L. (2021). Biphasic Activation of WNT Signaling Facilitates the Derivation of Midbrain Dopamine Neurons from hESCs for Translational Use. *Cell Stem Cell*, *28*(2), 343-355.e5. https://doi.org/10.1016/j.stem.2021.01.005

Kim, W. Y. (2012). NeuroD1 is an upstream regulator of NSCL1. *Biochemical and Biophysical Research Communications*, *419*(1), 27–31. https://doi.org/10.1016/J.BBRC.2012.01.100

Kirkeby, A., Nelander, J., Hoban, D. B., Paul, G., Barker, R. A., Parmar, M., Rogelius, N., Lmar Bjartmarz, H., Nordisk, N., Storm, P., Fiorenzano, A., Adler, A. F., Vale, S., Mudannayake, J., Zhang, Y., Cardoso, T., Mattsson, B., Landau, A. M., Glud, A. N., … Kan Widner, H. (2023). Clinical and Translational Report ll Clinical and Translational Report Preclinical quality, safety, and efficacy of a human embryonic stem cell-derived product for the treatment of Parkinson's disease, STEM-PD. *Stem Cell*, *30*, 1299-1314.e9. https://doi.org/10.1016/j.stem.2023.08.014

Kirkeby, A., Nelander, J., Hoban, D. B., Rogelius, N., Bjartmarz, H., Storm, P., Fiorenzano, A., Adler, A. F., Vale, S., Mudannayake, J., Zhang, Y., Cardoso, T., Mattsson, B., Landau, A. M., Glud, A. N., Sørensen, J. C., Lillethorup, T. P., Lowdell, M., Carvalho, C., … Parmar, M. (2023). Preclinical quality, safety, and efficacy of a human embryonic stem cell-derived product for the treatment of Parkinson's disease, STEM-PD. *Cell Stem Cell*, *30*(10), 1299-1314.e9. https://doi.org/10.1016/j.stem.2023.08.014

Koch, P., Opitz, T., Steinbeck, J. A., Ladewig, J., & Brüstle, O. (2009). A rosette-type, self-renewing human ES cell-derived neural stem cell with potential for in vitro instruction and synaptic integration. *Proceedings of the National Academy of Sciences of the United States of America*, *106*(9), 3225–3230. https://doi.org/10.1073/pnas.0808387106

Korsunsky, I., Millard, N., Fan, J., Slowikowski, K., Zhang, F., Wei, K., Baglaenko, Y., Brenner, M., Loh, P. ru, & Raychaudhuri, S. (2019). Fast, sensitive, and accurate integration of single cell data with Harmony. *Nature Methods*, *16*(12), 1289. https://doi.org/10.1038/S41592-019-0619-0

Kriks, S., Shim, J.-W., Piao, J., Ganat, Y. M., Wakeman, D. R., Xie, Z., Carrillo-Reid, L., Auyeung, G., Antonacci, C., Buch, A., Yang, L., Beal, M. F., Surmeier, D. J., Kordower, J. H., Tabar, V., & Studer, L. (2011). Dopamine neurons derived from human ES cells efficiently engraft in animal models of Parkinson's disease. *Nature*, *480*(7378), 547–551. https://doi.org/10.1038/nature10648

La Manno, G., Gyllborg, D., Codeluppi, S., Nishimura, K., Salto, C., Zeisel, A., Borm, L. E., Stott, S. R. W., Toledo, E. M., Villaescusa, J. C., Lönnerberg, P., Ryge, J., Barker, R. A., Arenas, E., & Linnarsson, S. (2016). Molecular Diversity of Midbrain Development in Mouse, Human, and Stem Cells. *Cell*, *167*(2), 566-580.e19. https://doi.org/10.1016/J.CELL.2016.09.027

Mannens, C. C. A., Hu, L., Lönnerberg, P., Schipper, M., Reagor, C. C., Li, X., He, X., Barker, R. A., Sundström, E., Posthuma, D., & Linnarsson, S. (2024). Chromatin accessibility during human first-trimester neurodevelopment. *Nature 2024*, 1–8. https://doi.org/10.1038/s41586-024-07234-1

McGinnis, C. S., Murrow, L. M., & Gartner, Z. J. (2019). DoubletFinder: Doublet Detection in Single-Cell RNA Sequencing Data Using Artificial Nearest Neighbors. *Cell Systems*, *8*(4), 329-337.e4. https://doi.org/10.1016/j.cels.2019.03.003

Mesman, S., Wever, I., & Smidt, M. P. (2021). Tcf4 Is Involved in Subset Specification of Mesodiencephalic Dopaminergic Neurons. *Biomedicines 2021, Vol. 9, Page 317*, *9*(3), 317. https://doi.org/10.3390/BIOMEDICINES9030317

Murdoch, J. N., Eddleston, J., Leblond-Bourget, N., Stanier, P., & Copp, A. J. (1999). Sequence and expression analysis of Nhlh1: a basic helix-loop-helix gene implicated in neurogenesis. *Developmental Genetics*, *24*(1–2), 165–177. https://doi.org/10.1002/(SICI)1520-6408(1999)24:1/2<165::AID-DVG15>3.0.CO;2-V

Nakamura, H., Katahira, T., Matsunaga, E., & Sato, T. (2005). Isthmus organizer for midbrain and hindbrain development. *Brain Research Reviews*, *49*(2), 120–126. https://doi.org/10.1016/J.BRAINRESREV.2004.10.005

Nie, S., Li, B., Wang, M., Chen, Z., Ren, J., Li, Z., Xu, X., Qian, Z., Xie, Z., Han, J., Zhang, Z., Zhang, Z., Zhu, Y., Chen, Z., Yang, X., & Ye, K. (2025). Sox6 and ALDH1A1 Truncation by Asparagine Endopeptidase Defines Selective Neuronal Vulnerability in Parkinson's Disease. *Advanced Science*, *12*(2), 2409477. https://doi.org/10.1002/ADVS.202409477

Nishimura, K., Ásgrímsdóttir, E. S., Yang, S., & Arenas, E. (2023). A protocol for the differentiation of human embryonic stem cells into midbrain dopaminergic neurons. *STAR Protocols*, *4*(3), 102355. https://doi.org/10.1016/J.XPRO.2023.102355

Nishimura, K., Yang, S., Lee, K. W., Ásgrímsdóttir, E. S., Nikouei, K., Paslawski, W., Gnodde, S., Lyu, G., Hu, L., Saltó, C., Svenningsson, P., Hjerling-Leffler, J., Linnarsson, S., & Arenas, E. (2023). Single-cell transcriptomics reveals correct developmental dynamics and high-quality midbrain cell types by improved hESC differentiation. *Stem Cell Reports*, *18*(1), 337–353. https://doi.org/10.1016/J.STEMCR.2022.10.016

Nürnberg, E., Horschitz, S., Schloss, P., & Meyer-Lindenberg, A. (2018). Basal glucocorticoid receptor activation induces proliferation and inhibits neuronal differentiation of human induced pluripotent stem cell-derived neuronal precursor cells. *The Journal of Steroid*

991 *Biochemistry and Molecular Biology*, *182*, 119–126.
992 https://doi.org/10.1016/J.JSBMB.2018.04.017

993 Oosterveen, T., Garção, P., Moles-Garcia, E., Soleilhavoup, C., Travaglio, M., Sheraz, S., Peltrini,
994 R., Patrick, K., Labas, V., Combes-Soia, L., Marklund, U., Hohenstein, P., & Panman, L.
995 (2021). Pluripotent stem cell derived dopaminergic subpopulations model the selective
996 neuron degeneration in Parkinson's disease. *Stem Cell Reports*, *16*(11), 2718–2735.
997 https://doi.org/10.1016/j.stemcr.2021.09.014

998 Pantazis, C. B., Yang, A., Lara, E., McDonough, J. A., Blauwendraat, C., Peng, L., Oguro, H.,
999 Kanaujiya, J., Zou, J., Sebesta, D., Pratt, G., Cross, E., Blockwick, J., Buxton, P., Kinner-
1000 Bibeau, L., Medura, C., Tompkins, C., Hughes, S., Santiana, M., ... Merkle, F. T. (2022). A
1001 reference human induced pluripotent stem cell line for large-scale collaborative studies.
1002 *Cell Stem Cell*, *29*(12), 1685-1702.e22. https://doi.org/10.1016/J.STEM.2022.11.004

1003 Piao, J., Zabierowski, S., Dubose, B. N., Hill, E. J., Navare, M., Claros, N., Rosen, S., Ramnarine,
1004 K., Horn, C., Fredrickson, C., Wong, K., Safford, B., Kriks, S., El Maarouf, A., Rutishauser, U.,
1005 Henchcliffe, C., Wang, Y., Riviere, I., Mann, S., ... Tabar, V. (2021). Preclinical Efficacy and
1006 Safety of a Human Embryonic Stem Cell-Derived Midbrain Dopamine Progenitor Product,
1007 MSK-DA01. *Cell Stem Cell*, *28*(2), 217-229.e7. https://doi.org/10.1016/j.stem.2021.01.004

1008 Pissadaki, E. K., & Bolam, J. P. (2013). The energy cost of action potential propagation in
1009 dopamine neurons: clues to susceptibility in Parkinson's disease. *Frontiers in*
1010 *Computational Neuroscience*, *7*(FEB). https://doi.org/10.3389/FNCOM.2013.00013

1011 Poewe, W., Seppi, K., Tanner, C. M., Halliday, G. M., Brundin, P., Volkmann, J., Schrag, A. E., &
1012 Lang, A. E. (2017). Parkinson disease. *Nature Reviews Disease Primers 2017 3:1*, *3*(1), 1–21.
1013 https://doi.org/10.1038/nrdp.2017.13

1014 Poulin, J. F., Caronia, G., Hofer, C., Cui, Q., Helm, B., Ramakrishnan, C., Chan, C. S., Dombeck,
1015 D. A., Deisseroth, K., & Awatramani, R. (2018). Mapping projections of molecularly defined
1016 dopamine neuron subtypes using intersectional genetic approaches. *Nature Neuroscience*
1017 *2018 21:9*, *21*(9), 1260–1271. https://doi.org/10.1038/s41593-018-0203-4

1018 Prakash, N., Brodski, C., Naserke, T., Puelles, E., Gogoi, R., Hall, A., Panhuysen, M., Echevarria,
1019 D., Sussel, L., Vogt Weisenhorn, D. M., Martinez, S., Arenas, E., Simeone, A., & Wurst, W.
1020 (2006). A Wnt1-regulated genetic network controls the identity and fate of midbrain-
1021 dopaminergic progenitors in vivo. *Development*, *133*(1), 89–98.
1022 https://doi.org/10.1242/DEV.02181

1023 Puelles, E., Annino, A., Tuorto, F., Usiello, A., Acampora, D., Czerny, T., Brodski, C., Ang, S. L.,
1024 Wurst, W., & Simeone, A. (2004). Otx2 regulates the extent, identity and fate of neuronal
1025 progenitor domains in the ventral midbrain. *Development*, *131*(9), 2037–2048.
1026 https://doi.org/10.1242/DEV.01107

1027 Rekaik, H., Blaudin De Thé, F. X., Prochiantz, A., Fuchs, J., & Joshi, R. L. (2015). Dissecting the
1028 role of Engrailed in adult dopaminergic neurons – Insights into Parkinson disease
1029 pathogenesis. *FEBS Letters*, *589*(24PartA), 3786–3794.
1030 https://doi.org/10.1016/J.FEBSLET.2015.10.002

1031 Satpathy, A. T., Granja, J. M., Yost, K. E., Qi, Y., Meschi, F., McDermott, G. P., Olsen, B. N.,
1032 Mumbach, M. R., Pierce, S. E., Corces, M. R., Shah, P., Bell, J. C., Jhutty, D., Nemec, C. M.,

Wang, J., Wang, L., Yin, Y., Giresi, P. G., Chang, A. L. S., … Chang, H. Y. (2019). Massively parallel single-cell chromatin landscapes of human immune cell development and intratumoral T cell exhaustion. *Nature Biotechnology 2019 37:8*, *37*(8), 925–936. https://doi.org/10.1038/s41587-019-0206-z

Sawamoto, N., Doi, D., Nakanishi, E., Sawamura, M., Kikuchi, T., Yamakado, H., Taruno, Y., Shima, A., Fushimi, Y., Okada, T., Kikuchi, T., Morizane, A., Hiramatsu, S., Anazawa, T., Shindo, T., Ueno, K., Morita, S., Arakawa, Y., Nakamoto, Y., … Takahashi, J. (2025). Phase I/II trial of iPS-cell-derived dopaminergic cells for Parkinson's disease. *Nature 2025 641:8064*, *641*(8064), 971–977. https://doi.org/10.1038/s41586-025-08700-0

Schweitzer, J. S., Song, B., Herrington, T. M., Park, T.-Y., Lee, N., Ko, S., Jeon, J., Cha, Y., Kim, K., Li, Q., Henchcliffe, C., Kaplitt, M., Neff, C., Rapalino, O., Seo, H., Lee, I.-H., Kim, J., Kim, T., Petsko, G. A., … Kim, K.-S. (2020). Personalized iPSC-Derived Dopamine Progenitor Cells for Parkinson's Disease. *The New England Journal of Medicine*, *382*(20), 1926–1932. https://doi.org/10.1056/NEJMoa1915872

Sharma, Y., Saha, S., Joseph, A., Krishnan, H., & Raghu, P. (2020). In vitro human stem cell derived cultures to monitor calcium signaling in neuronal development and function. *Wellcome Open Research*, *5*. https://doi.org/10.12688/WELLCOMEOPENRES.15626.1

Sif Ásgrímsdóttir, E., Fusar Bassini, L., Rivetti, P., Cervo, V., Gyllborg, D., Puigsasllosas Pastor, C., Lee, K., Grigsby, C., Islam, S., Lönneberg, P., Villaescusa, C., Saltó, C., Linnarsson, S., Manno, G. La, Toledo, E. M., & Arenas, E. (2024). Midbrain Dopaminergic Neuron Development is Regulated by Two Molecularly Distinct Subtypes of Radial Glia Cells. *BioRxiv*, 2024.03.08.584031. https://doi.org/10.1101/2024.03.08.584031

Siletti, K., Hodge, R., Mossi Albiach, A., Lee, K. W., Ding, S.-L., Hu, L., Lönnerberg, P., Bakken, T., Casper, T., Clark, M., Dee, N., Gloe, J., Hirschstein, D., Shapovalova, N. V, Keene, C. D., Nyhus, J., Tung, H., Yanny, A. M., Arenas, E., … Linnarsson, S. (2023). Transcriptomic diversity of cell types across the adult human brain. *Science (New York, N.Y.)*, *382*(6667), eadd7046. https://doi.org/10.1126/science.add7046

Simon, H. H., Saueressig, H., Wurst, W., Goulding, M. D., & O'Leary, D. D. M. (2001). Fate of Midbrain Dopaminergic Neurons Controlled by the Engrailed Genes. *Journal of Neuroscience*, *21*(9), 3126–3134. https://doi.org/10.1523/JNEUROSCI.21-09-03126.2001

Smidt, M. P., Smits, S. M., Bouwmeester, H., Hamers, F. P. T., van der Linden, A. J. A., Hellemons, A. J. C. G. M., Graw, J., & Burbach, J. P. H. (2004). Early developmental failure of substantia nigra dopamine neurons in mice lacking the homeodomain gene Pitx3. *Development*, *131*(5), 1145–1155. https://doi.org/10.1242/DEV.01022

Stuart, T., Butler, A., Hoffman, P., Hafemeister, C., Papalexi, E., Mauck, W. M., Hao, Y., Stoeckius, M., Smibert, P., & Satija, R. (2019). Comprehensive Integration of Single-Cell Data. *Cell*, *177*(7), 1888-1902.e21. https://doi.org/10.1016/j.cell.2019.05.031

Stuart, T., Srivastava, A., Madad, S., Lareau, C. A., & Satija, R. (2021). Single-cell chromatin state analysis with Signac. *Nature Methods 2021 18:11*, *18*(11), 1333–1341. https://doi.org/10.1038/s41592-021-01282-5

Tabar, V., Sarva, H., Lozano, A. M., Fasano, A., Kalia, S. K., Yu, K. K. H., Brennan, C., Ma, Y., Peng, S., Eidelberg, D., Tomishima, M., Irion, S., Stemple, W., Abid, N., Lampron, A., Studer, L., &

Henchcliffe, C. (2025). Phase I trial of hES cell-derived dopaminergic neurons for Parkinson's disease. *Nature 2025 641:8064*, *641*(8064), 978–983. https://doi.org/10.1038/s41586-025-08845-y

Takahashi, J. (2020). iPS cell-based therapy for Parkinson's disease: A Kyoto trial. *Regenerative Therapy*, *13*, 18–22. https://doi.org/10.1016/J.RETH.2020.06.002

Tang, L., Xu, N., Huang, M., Yi, W., Sang, X., Shao, M., Li, Y., Hao, Z. zhe, Liu, R., Shen, Y., Yue, F., Liu, X., Xu, C., & Liu, S. (2023). A primate nigrostriatal atlas of neuronal vulnerability and resilience in a model of Parkinson's disease. *Nature Communications 2023 14:1*, *14*(1), 1–13. https://doi.org/10.1038/s41467-023-43213-2

Theofilopoulos, S., Wang, Y., Kitambi, S. S., Sacchetti, P., Sousa, K. M., Bodin, K., Kirk, J., Saltó, C., Gustafsson, M., Toledo, E. M., Karu, K., Gustafsson, J. Å., Steffensen, K. R., Ernfors, P., Sjövall, J., Griffiths, W. J., & Arenas, E. (2012). Brain endogenous liver X receptor ligands selectively promote midbrain neurogenesis. *Nature Chemical Biology 2012 9:2*, *9*(2), 126–133. https://doi.org/10.1038/nchembio.1156

Thibodeau, A., Eroglu, A., McGinnis, C. S., Lawlor, N., Nehar-Belaid, D., Kursawe, R., Marches, R., Conrad, D. N., Kuchel, G. A., Gartner, Z. J., Banchereau, J., Stitzel, M. L., Cicek, A. E., & Ucar, D. (2021). AMULET: a novel read count-based method for effective multiplet detection from single nucleus ATAC-seq data. *Genome Biology*, *22*(1), 252. https://doi.org/10.1186/s13059-021-02469-x

iklová, K., Björklund, Å. K., Lahti, L., Fiorenzano, A., Nolbrant, S., Gillberg, L., Volakakis, N., Yokota, C., Hilscher, M. M., Hauling, T., Holmström, F., Joodmardi, E., Nilsson, M., Parmar, M., & Perlmann, T. (2019). Single-cell RNA sequencing reveals midbrain dopamine neuron diversity emerging during mouse brain development. *Nature Communications 2019 10:1*, *10*(1), 1–12. https://doi.org/10.1038/s41467-019-08453-1

Tiklová, K., Nolbrant, S., Fiorenzano, A., Björklund, Å. K., Sharma, Y., Heuer, A., Gillberg, L., Hoban, D. B., Cardoso, T., Adler, A. F., Birtele, M., Lundén-Miguel, H., Volakakis, N., Kirkeby, A., Perlmann, T., & Parmar, M. (2020). Single cell transcriptomics identifies stem cell-derived graft composition in a model of Parkinson's disease. *Nature Communications*, *11*(1). https://doi.org/10.1038/S41467-020-16225-5

Toledo, E. M., Yang, S., Gyllborg, D., van Wijk, K. E., Sinha, I., Varas-Godoy, M., Grigsby, C. L., Lönnerberg, P., Islam, S., Steffensen, K. R., Linnarsson, S., & Arenas, E. (2020). Srebf1 Controls Midbrain Dopaminergic Neurogenesis. *Cell Reports*, *31*(5), 107601. https://doi.org/10.1016/j.celrep.2020.107601

Tolve, M., Ulusoy, A., Patikas, N., Islam, K. U. S., Bodea, G. O., Öztürk, E., Broske, B., Mentani, A., Wagener, A., van Loo, K. M. J., Britsch, S., Liu, P., Khaled, W. T., Metzakopian, E., Baader, S. L., Di Monte, D. A., & Blaess, S. (2021). The transcription factor BCL11A defines distinct subsets of midbrain dopaminergic neurons. *Cell Reports*, *36*(11), 109697. https://doi.org/10.1016/j.celrep.2021.109697

Trapnell, C., Cacchiarelli, D., Grimsby, J., Pokharel, P., Li, S., Morse, M., Lennon, N. J., Livak, K. J., Mikkelsen, T. S., & Rinn, J. L. (2014). The dynamics and regulators of cell fate decisions are revealed by pseudotemporal ordering of single cells. *Nature Biotechnology 2014 32:4*, *32*(4), 381–386. https://doi.org/10.1038/nbt.2859

Xi, J., Liu, Y., Liu, H., Chen, H., Emborg, M. E., & Zhang, S. C. (2012). Specification of Midbrain Dopamine Neurons from Primate Pluripotent Stem Cells. *Stem Cells*, *30*(8), 1655–1663. https://doi.org/10.1002/STEM.1152

Xu, C., Prete, M., Webb, S., Jardine, L., Stewart, B. J., Hoo, R., He, P., Meyer, K. B., & Teichmann, S. A. (2023). Automatic cell-type harmonization and integration across Human Cell Atlas datasets. *Cell*, *186*(26), 5876-5891.e20. https://doi.org/10.1016/j.cell.2023.11.026

Xu, P., He, H., Gao, Q., Zhou, Y., Wu, Z., Zhang, X., Sun, L., Hu, G., Guan, Q., You, Z., Zhang, X., Zheng, W., Xiong, M., & Chen, Y. (2022). Human midbrain dopaminergic neuronal differentiation markers predict cell therapy outcomes in a Parkinson's disease model. *The Journal of Clinical Investigation*, *132*(14). https://doi.org/10.1172/JCI156768

Yaghmaeian Salmani, B., Lahti, L., Gillberg, L., Jacobsen, J. K., Mantas, I., Svenningsson, P., & Perlmann, T. (2024). Transcriptomic atlas of midbrain dopamine neurons uncovers differential vulnerability in a Parkinsonism lesion model. *ELife*, *12*. https://doi.org/10.7554/ELIFE.89482

Zetterström, R. H., Solomin, L., Jansson, L., Hoffer, B. J., Olson, L., & Perlmann, T. (1997). Dopamine Neuron Agenesis in Nurr1-Deficient Mice. *Science*, *276*(5310), 248–250. https://doi.org/10.1126/SCIENCE.276.5310.248

Zhang, D., Yang, S., Toledo, E. M., Gyllborg, D., Saltó, C., Carlos Villaescusa, J., & Arenas, E. (2017). Niche-derived laminin-511 promotes midbrain dopaminergic neuron survival and differentiation through YAP. *Science Signaling*, *10*(493). https://doi.org/10.1126/scisignal.aal4165

Zhang, Y., Liu, T., Meyer, C. A., Eeckhoute, J., Johnson, D. S., Bernstein, B. E., Nusbaum, C., Myers, R. M., Brown, M., Li, W., & Liu, X. S. (2008). Model-based analysis of ChIP-Seq (MACS). *Genome Biology*, *9*(9), R137. https://doi.org/10.1186/gb-2008-9-9-r137

Zheng, G. X. Y., Terry, J. M., Belgrader, P., Ryvkin, P., Bent, Z. W., Wilson, R., Ziraldo, S. B., Wheeler, T. D., McDermott, G. P., Zhu, J., Gregory, M. T., Shuga, J., Montesclaros, L., Underwood, J. G., Masquelier, D. A., Nishimura, S. Y., Schnall-Levin, M., Wyatt, P. W., Hindson, C. M., … Bielas, J. H. (2017). Massively parallel digital transcriptional profiling of single cells. *Nature Communications 2017 8:1*, *8*(1), 1–12. https://doi.org/10.1038/ncomms14049

Zhou, Y., Zhou, B., Pache, L., Chang, M., Khodabakhshi, A. H., Tanaseichuk, O., Benner, C., & Chanda, S. K. (2019). Metascape provides a biologist-oriented resource for the analysis of systems-level datasets. *Nature Communications*, *10*(1), 1523. https://doi.org/10.1038/S41467-019-09234-6

Ziegler, A. B., Thiele, C., Tenedini, F., Richard, M., Leyendecker, P., Hoermann, A., Soba, P., & Tavosanis, G. (2017). Cell-Autonomous Control of Neuronal Dendrite Expansion via the Fatty Acid Synthesis Regulator SREBP. *Cell Reports*, *21*(12), 3346–3353. https://doi.org/10.1016/j.celrep.2017.11.069